JOURNAL OF COMPUTATIONAL PHYSICS 45, 157–209 (1982)

Nonlinear Normal Modes for the Toda Chain

W. E. FERGUSON, JR.

Department of Mathematics, Southern Methodist University, Dallas, Texas 75275

H. FLASCHKA* AND D. W. MCLAUGHLIN*

Department of Mathematics, University of Arizona, Tucson, Arizona 85721

Received March 30, 1981

The Toda Chain is a nonlinear mass–spring chain which can in principle be integrated analytically by the action-angle theory of classical mechanics. We show that the transformation from physical variables to action variables can be implemented very simply on a computer. We study the correspondence between action variables and the motions of the chain, and find the role of the action variables to be very similar to the role of normal-mode amplitudes in the harmonic chain. This similarity leads to a partly rigorous, partly heuristic normal-mode analysis for the Toda chain. New results are obtained when this normal-mode analysis is applied to certain perturbations of the Toda chain such as the Fermi–Pasta–Ulam chain or the Toda chain with a mass impurity.

1. INTRODUCTION

The motion of a chain of unit masses connected by identical springs is governed by the equations

$$q_n'' = F(\Delta q_{n-1}) - F(\Delta q_n), \tag{1.1}$$

where q_n is the displacement of the nth mass, measured from a fixed reference equilibrium position, and

$$\Delta q_n = q_{n+1} - q_n,$$
$$F(x) = -V'(x),$$

where $V(x)$ is the potential energy stored in a spring when its length is increased by an amount x. A complete analytical solution of (1.1) is known in only two cases. The most thoroughly studied case is the harmonic chain, with

$$V(x) = \tfrac{1}{2}x^2;$$

* Work supported in part by NSF Grants MCS 75-07530(-A01), MCS-7903533, and U.S. Army Contract DAAG 29-78-G-0059 and DAAG 29-81-K-0025.

0021-9991/82/020157-53$02.00/0

Copyright © 1982 by Academic Press, Inc.
All rights of reproduction in any form reserved.

its solution is obtained by using the discrete Fourier transform to represent the general solution as a *linear* superposition of (sinusiodal) normal modes. The second case is the Toda chain, with

$$V(x) = \frac{1}{\beta^2}\,[\exp(-\beta x) - (1 - \beta x)],$$

which was invented around 1967 [1] and solved in 1973 [2, 3] (independently in [4]); its solution is obtained by using a complicated transformation from q_n and q_n' to new variables.

Our aim in this paper is to show how the complicated transformation used to solve the Toda chain can be converted into a practical computational tool for the analysis of the motion of the Toda chain. We argue that this transformation allows one to view the general solution of the Toda chain as a *nonlinear* superposition of normal modes, an approach which yields a surprisingly detailed understanding of the behavior of the Toda chain. For small-amplitude motions of the Toda chain these normal modes are approximately the sinusoidal traveling waves of the harmonic chain; for large-amplitude motion of the Toda chain, the normal modes tend to the "soliton" solutions of the infinite Toda chain.

There are many reasons for studying the Toda chain. Most frequently it is used as a model of a one-dimensional solid. In this application the adjustable parameter "β" in V allows the corresponding force law

$$F(x) = \frac{1}{\beta}\,[\exp(-\beta x) - 1] \tag{1.2}$$

to approximate the harmonic force law as $\beta \to 0$, or the hard-core collision as $\beta \to +\infty$. It is known that (1.1) can be solved analytically (in terms of many-variable θ-functions) for all $\beta \in (0, \infty)$. In this respect the Toda chain is atypical; nowadays it is understood that "most" chains with nearest neighbor interactions have motions which exhibit at least some stochastic behavior. Still, the Toda chain is a convenient model for the study of the apparently ubiquitous soliton solutions of one-dimensional chains. For instance, it has recently been used as a test case for the analysis of shock waves in discrete nonlinear solids [5, 6]. In computer experiments, the motions of chains with various force laws, including the Toda force law, were found to be qualitatively similar; it is therefore natural to study shocks in a discrete chain by using the integrable Toda chain as a model. Indeed, a phenomenological analysis has been carried out with the methods of the present paper [7, 8].

Specific physical applications aside, the Toda chain occupies a unique position in the theory of nonlinear oscillators. It is one of the few systems which can be solved by the action-angle theory of classical dynamics. This venerable theory has not led to very many results, not only because integrable systems are hard to find, but also because the transformations required are difficult to implement. We will show that the action variables for the Toda chain can be displayed graphically using but a few seconds of computer time. This makes it possible to correlate the action variables

with the qualitative features of the motion of the chain. As a result, we have the *first* example of a nonlinear system with many degrees of freedom for which it is possible, and computationally inexpensive, to obtain all of the constants of the motion, and to predict from these constants the qualitative features of the subsequent motion of the system.

To see why this is useful, consider the harmonic chain whose action variables are related to the amplitudes of the various sinusoidal traveling-waves. The knowledge of these action variables (normal-mode amplitudes) allows one to describe qualitative features of the motion of the harmonic chain without integrating its equations of motion. Moreover, the analysis of the weak coupling of these action variables when the force law is only approximately harmonic has been a standard technique of physicists. We will show that these methods for the harmonic chain have analogs for the Toda chain.

Let us now describe the steps we use to analyze the qualitative features of the motion of the Toda chain. From given initial conditions we compute the amplitudes (values of the action variables) of the various normal modes of the Toda chain; these amplitudes remain constant throughout the chain's motion. Partly by theory, and partly by numerical experiment, we derive some rules which relate these initial amplitudes to the qualitative features of the subsequent motion of the chain.

The rest of the paper is organized as follows. The solution of the harmonic chain is reviewed in Section 2. Sections 3 and 4 present a very brief outline of the action–angle theory of Hamiltonian dynamics; in particular, we show how to compute the normal-mode amplitudes for the Toda chain. We try to provide the reader with an operational understanding of the revelant theory; for some details we refer to the original theoretical literature. In Section 5 we use "practice problems" to derive the rules which relate the normal-mode amplitudes to the qualitative features of the corresponding motion of the Toda chain. In particular, we investigate certain motions that result from prescribed normal-mode amplitudes; in some cases this involves the numerical solution of an inverse spectral problem as described in [9]. In Sections 6 and 7 we show how this nonlinear normal-mode analysis leads to new interpretations of the Fermi–Pasta–Ulam experiment [10], Zabusky's lattice soliton experiment [11], and the motion of the Toda chain when the value of one of its masses is changed.

Some of the results of this paper were presented at conferences on "Inverse Spectral Transforms" (Rome, 1977) and on "Nonlinear Waves" (Kyoto, 1978) [12].

2. The Harmonic Chain

In this paper we will typically be concerned with N-mass chains whose equations of motion are

$$q_n'' = F(\Delta q_{n-1}) - F(\Delta q_n), \qquad \text{for} \quad n = 1, 2, \ldots, N. \tag{2.1}$$

The N-mass fixed-end chain is obtained by imposing the boundary conditions

$$q_0 = 0 \qquad \text{and} \qquad q_{N+1} = 0, \tag{2.2}$$

while the N-mass periodic chain is obtained by imposing the boundary conditions

$$q_0 = q_N \qquad \text{and} \qquad q_{N+1} = q_1. \tag{2.3}$$

Without loss of generality we will consider only periodic chains; the N-mass fixed-end chain can be treated as a $(2N+2)$-mass periodic chain if one extends q_n, p_n as odd functions, e.g.,

$$q_{n+N+1} = -q_n \qquad \text{for} \quad n = 1, 2, \ldots, N+1$$

and similarly for p_n; as time evolves, q_n and p_n remain odd functions.

Let us now review those aspects of the N-mass periodic harmonic chain which will be relevant to our discusion of the Toda chain. The Hamiltonian for the harmonic chain is

$$H(q, p) = \tfrac{1}{2} p^T p - \tfrac{1}{2} q^T S q.$$

Here $q^T = (q_1, \ldots, q_N)$, $p^T = (p_1, \ldots, p_N)$, where T denotes transpose and

$$S = \begin{bmatrix} -2 & 1 & & & 1 \\ 1 & -2 & 1 & & \\ & & \cdots & & \\ & & 1 & -2 & 1 \\ 1 & & & 1 & -2 \end{bmatrix}.$$

Let O be an orthogonal matrix which diagonalizes S,

$$O^T S O = \operatorname{diag}(-\omega_1^2, \ldots, -\omega_N^2),$$
$$\omega_j = 2 \sin(k_j/2), \qquad k_j = 2\pi j/N.$$

With $p = O^T \tilde{p}$, $q = O\tilde{q}$, we transform the Hamiltonian H to principal axes:

$$H = \tfrac{1}{2} \sum (\tilde{p}_j^2 + \omega_j^2 \tilde{q}_j^2). \tag{2.4}$$

This change of variables is canonical, and so the equations of motion are

$$\tilde{q}_j' = \tilde{p}_j, \qquad \tilde{p}_j' = -\omega_j^2 \tilde{q}_j,$$

which are easily solved:

$$\tilde{q}_j = c_j \sin(\omega_j t + \theta_j^0), \qquad \tilde{q}_N = c_N t + \theta_N^0. \tag{2.5}$$

A solution for which the integration constants c_j vanish except for $j = m$ is commonly said to represent the mth normal mode. Because the eigenvalues $-\omega_j^2$ of S are double ($-\omega_N^2$ and $-\omega_{N/2}^2$ excepted), O is not unique, and the normal modes may appear as standing waves or as traveling waves. For comparison with the Toda chain, we choose the latter.

The *harmonic normal modes* are

$$q_n^{(m)} = \sqrt{\frac{2}{N}} \frac{1}{\omega_m} \sin(k_m n + \omega_m t + \theta_m^0), \qquad 1 \leqslant m \leqslant N-1,$$
$$q_n^{(N)} = \sqrt{2}\, t + \theta_N^0; \tag{2.6}$$

here

$$k_m = \frac{2\pi m}{N}, \qquad \omega_m = 2 \sin\left(\frac{k_m}{2}\right).$$

Observe that $k_{N-j} = 2\pi - k_j$ while $\omega_{N-j} = \omega_j$. Thus $q^{(j)}$ represents a left-running wave and $q^{(N-j)}$ a right-running wave with wavenumber k_j for $j = 1,..., |(N-1)/2|$. If the general solution of the harmonic chain is written as

$$q = \sum_{m=1}^{N} A^{(m)} q^{(m)},$$

then the total energy is

$$H = \sum_{m=1}^{N} |A^{(m)}|^2.$$

We speak of $|A^{(m)}|^2$ as the energy contained in the mth normal mode. By (2.4) and (2.6), $|A^{(m)}|^2$ is proportional to $|c_m|^2$ in (2.5), which in turn is proportional to $\frac{1}{2}(\tilde{p}_m^2 + \omega_m^2 \tilde{q}_m^2)$ in (2.4).

The simple linear transformation from q, p to $\tilde{q}$, $\tilde{p}$ makes it very easy to obtain an analytic expression for the solution of the harmonic chain. It is equally important, however, that the normal-mode amplitudes $A^{(m)}$ also carry qualitative information about the motion of the chain. One can compute the normal-mode amplitudes $A^{(m)}$ from the initial data, and so one knows whether long waves or short waves are predominant in the chain's motion. Furthermore, various asymptotic calculations utilize the normal-mode amplitudes; for long chains a stationary phase approximation describes the large-time behavior of the motion, and for weakly nonlinear force laws the normal-mode amplitudes couple to each other and change slowly with time.

Our aim is to analyze the Toda chain, and chains which approximate the Toda chain, by a nonlinear version of normal mode theory. The analysis above relied heavily on the linearity of the harmonic chain and so it is not obvious how to extend it to the Toda chain. In the next section we present an alternate approach to the harmonic chain—one which does generalize to the Toda chain.

3. Action-Angle Variables

It is evident that each of the quantities

$$I_m = \tfrac{1}{2}(\tilde{p}_m^2 + \omega_m^2 \tilde{q}_m^2) \qquad \text{for} \quad m = 1,..., N \tag{3.1}$$

is a constant of the motion. Indeed, we have observed that I_m is the square of the mth normal mode amplitude $A^{(m)}$. Therefore the phase-space trajectory $(q(t), p(t))$ must lie on the surface S defined by

$$I_m(q, p) = I_m^0 \qquad \text{for} \quad m = 1,..., N, \tag{3.2}$$

where I_m^0 is the value of (3.1) determined from the initial conditions. The shape of the surface S is thus determined by the values of I_m^0 and is a geometric reflection of the relative sizes of the normal-mode amplitudes $A^{(m)}$. It will be convenient to think geometrically when we analyze the Toda lattice; so, let us develop our geometric intuition using the harmonic chain as an example.

Example 1. Suppose $I_m^0 = 0$ for $m = 1,..., N$. From (3.1) we infer that $\tilde{q}_m = \tilde{p}_m = 0$ for $m = 1, 2,..., N-1$ and $\tilde{p}_N = 0$. This implies that q is a constant and p is zero, i.e., S is a point. This obviously describes a state in which the chain is at rest.

Example 2. Suppose $I_m^0 = 0$ for $m = 1,..., N-1$ and $I_N^0 \neq 0$. From (3.1) we infer that $\tilde{q}_m = \tilde{p}_m = 0$ for $m = 1,..., N-1$ and $\tilde{p}_N \neq 0$. This implies that q increases linearly with time, while p is a constant, i.e., S is a straight line. This obviously describes a uniform translation of the chain.

Example 3. Suppose $I_1^0 \neq 0$ and $I_m^0 = 0$ for $m = 2,..., N$. The surface S is the ellipse

$$\tfrac{1}{2}(\tilde{p}_1^2 + \omega_1^2 \tilde{q}_1^2) = I_1^0,$$

which lies in the $\tilde{q}_1 - \tilde{p}_1$ plane. The area enclosed by the ellipse is $2\pi I_1^0/\omega_1$, a number proportional to the square of the normal-mode amplitude $A^{(1)}$.

Example 4. Suppose $I_1^0 \neq 0$, $I_2^0 \neq 0$ and $I_m^0 = 0$ for $m = 3,..., N$. The surface S is the two-dimensional torus

$$\tfrac{1}{2}(\tilde{p}_1^2 + \omega_1^2 \tilde{q}_1^2) = I_1^0,$$
$$\tfrac{1}{2}(\tilde{p}_2^2 + \omega_2^2 \tilde{q}_2^2) = I_2^0$$

which lies in the four-dimensional span of the $\tilde{q}_1 - \tilde{p}_1$ and $\tilde{q}_2 - \tilde{p}_2$ planes. The cross-sectional areas of this torus in the $\tilde{q}_1 - \tilde{p}_1$ and $\tilde{q}_2 - \tilde{p}_2$ planes are, respectively, $2\pi I_1^0/\omega_1$ and $2\pi I_2^0/\omega_2$; these numbers are proportional to the squares of the normal-mode amplitudes $A^{(1)}$ and $A^{(2)}$.

These examples illustrate the following general facts:

(1) The dimension of the surface S reflects the number of degrees of freedom (the number of normal modes having nonzero amplitudes) excited in the chain. The maximal dimension of the surface S defined by (3.2) is N (so only N normal modes can be excited).

(2) The surface S is the topological product of up to $N-1$ ellipses and 1 line. The line disappears if the center of mass does not move. If we ignore the center of mass motion, e.g., by using a center of mass coordinate system, then S can be considered to be a torus of dimension k where $0 \leqslant k \leqslant N-1$.

(3) The cross-sectional areas of the torus are proportional to the squares of the amplitudes of the excited normal modes. On a given torus of dimension at least 2, there are many different solution trajectories. Each trajectory on S is characterized by the same normal-mode amplitudes $A^{(m)}$, but the relative phases with which these normal modes are superimposed are different for different trajectories.

What we have just described is the geometry of action-angle variables for the harmonic chain. Let γ_i be the intersection of the torus S with the $q_i - p_i$ plane; γ_i is a curve which encircles S once in one of the $N-1$ "independent" directions (remember that the center-of-mass motion is being disregarded). The action variable J_i is defined by

$$J_i = \frac{1}{2\pi} \int_{\gamma_i} \sum_j \tilde{p}_j \, d\tilde{q}_j. \tag{3.3}$$

(One can check that

$$\sum \tilde{p}_j \, d\tilde{q}_j = \sum p_j \, dq_j + (\text{a perfect differential}),$$

so that one could equally well use the physical coordinates in (3.3).) Note that $\tilde{q}_i$ is constant on γ_j unless $j = i$, so that

$$J_i = \frac{1}{2\pi} \int_{\gamma_i} \tilde{p}_i \, d\tilde{q}_i. \tag{3.4}$$

Using

$$\tfrac{1}{2}(\tilde{p}_i^2 + \omega_i^2 \tilde{q}_i^2) = I_i^0,$$

we find that

$$J_i = I_i^0/\omega_i. \tag{3.5}$$

The examples above show that (*for the harmnoic chain*, at least), *the J_i are measures of the cross-sectional areas of the torus S in the various independent coordinate directions.*

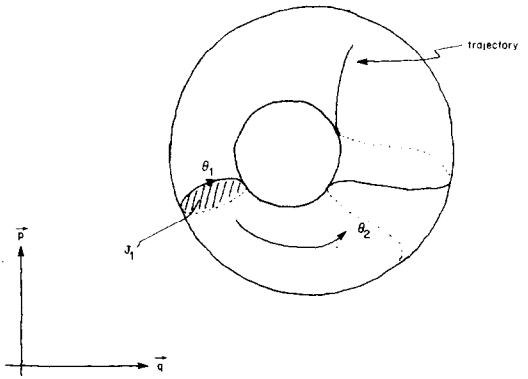

FIG. 1. A schematic drawing of an invariant torus.

In the action-angle theory of mechanics, one introduces, along with the actions J_i, a set of angle coordinates θ_i, $0 \leqslant \theta_i \leqslant 2\pi$. The phase-space is filled out by tori $I_i = I_i^0$. The transformation $(q, p) \to (\theta, J)$

(i) places the point (q, p) on a torus characterized by the values J_i, via $I_i(q, p) = \omega_i J_i$, and

(ii) locates the point (q, p) on this torus by specifying the angular coordinates θ_i (see Fig. 1 for a schematic drawing).

It is possible to make the transformation *canonical*, i.e., the equations of motion become

$$\theta_i' = \frac{\partial H}{\partial J_i}, \qquad J_i' = -\frac{\partial H}{\partial \theta_i}.$$

From (2.4), (2.6), (3.5) we find

$$H = \sum_i \omega_i J_i,$$

so

$$\theta_i' = \omega_i, \qquad J_i' = 0,$$

and it is easily checked that this agrees with the normal-mode solution (2.5).

For details of this theory, see [13]. The main point is that the harmonic normal modes are obtained by a purely geometric method, relying in no way on the linearity of the equations of motion. A standard theorem of mechanics [13] gives conditions under which this picture applies to more general Hamiltonian systems.

Let the Hamiltonian equations

$$q_n' = \frac{\partial H}{\partial p_n}, \qquad p_n' = -\frac{\partial H}{\partial q_n} \qquad \text{for} \quad n = 1,..., N,$$

admit N constants of the motion which are functionally independent and mutually in involution (i.e., their Poisson brackets $\{I_m, I_n\} \equiv \sum_i ((\partial I_n/\partial p_i)(\partial I_m/\partial q_i) - (\partial I_n/\partial q_i)(\partial I_m/\partial p_i))$ vanish). If a solution of these equations has constants of motion $I_n(q(t), p(t)) = I_n^0$, its trajectory $(q(t), p(t))$ winds around the surface S defined by

$$I_n(q, p) = I_n^0 \qquad \text{for} \quad n = 1,..., N,$$

which can always be viewed as a topological product of circles and lines. If we ignore these lines (in our case there is only one line and this line describes a uniform translation of the chain), then S is a torus. As before, the dimension of this torus is a measure of the number of excited degrees of freedom. For example, if the dimension of S is 0, the trajectory is a point and the chain is at rest. If the dimension of S is 1, the trajectory is a closed curve and the solution is periodic in time.

As in the harmonic case, one can now change from the original coordinates (q, p) via a canonical transformation to action-angle coordinates (θ, J). For the Toda chain, two of these coordinates, say θ_N and J_N, describe the center of mass motion; J_N characterizes the chain's total momentum and θ_N characterizes the chain's center of mass. The remaining action variables $J_1,..., J_{N-1}$ define the torus S, while the angle variables $\theta_1,..., \theta_{N-1}$ provide a coordinate system on S.

As before, the actions J_i for $i = 1,..., N-1$ are given by (3.3). In the harmonic case, the paths γ_i were explicitly coordinatized. In a more general Hamiltonian system possessing N integrals in involution, the γ_i are known to exist by abstract topological arguments; this is not enough to guarantee that the line integrals (3) can actually be evaluated. The theory of the periodic Toda chain [14], however, provides:

(i) an explicit parametrization of the curves γ_i, so that the integrals (3.3) are perfectly concrete,

(ii) a new set of canonical coordinates $\tilde{q}_i$, $\tilde{p}_i$ in terms of which the integrand $\sum \tilde{p}_i d\tilde{q}_i$ of (3.3) reduces to $\tilde{p}_j d\tilde{q}_j$ on γ_j ($\tilde{q}_i$ is constant on γ_j when $i \neq j$). So (3.3) simplifies to (3.4), and the computation of the action variables reduces to the evaluation of a *planar* line integral.

The Toda chain is the first, and still the only, large nonlinear system of physical interest for which the theoretical action-angle prescription can be converted into a concrete computational problem. The needed integrals (3.4) are still so complex [14] that one could not expect to derive much qualitative information from the numerical evaluation alone. We show in the next section that the values of the action-variable integrals (3.4) may be pictured very simply as areas under portions of a certain curve computed easily from the initial conditions.

Our strategy in this paper will be as follows. From given initial conditions plot the graph which, according to the hints above, displays the action variables as areas; then relate the actions to the motion of the chain in a way reminiscent of the use of harmonic normal modes in the qualitative description of the harmonic chain. It may seem that this sort of interpretation of action variables as nonlinear normal-mode amplitudes is very obvious, especially when one considers the standard identification

of linear normal modes with harmonic action variables; if there were any content to the analogy, it should perhaps have been exploited by now. This is not the case, simply because the validity of any analogy between nonlinear action variables and linear normal-mode amplitudes could not be investigated without an efficient way to compute the actions, and this has only recently become available.

4. Phase-Space Geometry of the Toda Chain

Let us now outline how the previously described theory is applied to the Toda chain.

We begin with the equations of motion for the N-mass periodic Toda chain:

$$q_n' = p_n, \qquad p_n' = F(\Gamma + \Delta q_{n-1}) - F(\Gamma + \Delta q_n) \qquad \text{for} \quad n = 1,\ldots, N, \tag{4.1}$$

where

$$F(x) = \frac{1}{\beta}\,[\exp(-\beta x) - 1], \qquad q_0 = q_N \quad \text{and} \quad q_{N+1} = q_1. \tag{4.2}$$

Here Γ represents the amount by which each spring is extended from its natural length when the chain is at rest. Γ would be nonzero if the chain is subjected to external pressure, which is the case in some applications [7]. Define

$$a_n = \frac{1}{2}\exp\left(-\frac{\beta}{2}\,[\Gamma + \Delta q_n]\right), \qquad b_n = \frac{\beta}{2}\,p_n \qquad \text{for} \quad n = 1,\ldots, N \tag{4.3}$$

and observe that the equations of motion (4.1) take the form

$$a_n' = a_n(b_{n+1} - b_n), \qquad b_n' = 2(a_n^2 - a_{n-1}^2) \qquad \text{for} \quad n = 1,\ldots, N, \tag{4.4}$$

where obviously

$$a_0 = a_N \qquad \text{and} \qquad b_{N+1} = b_1.$$

Crucial for all later development is the following periodic Jacobi matrix:

$$L = \begin{bmatrix} b_1 & a_1 & & & a_N \\ a_1 & b_2 & a_2 & 0 & \\ & & \cdots & & \\ & 0 & a_{N-2} & b_{N-1} & a_{N-1} \\ a_N & & & a_{N-1} & b_N \end{bmatrix}.$$

The entries of L depend on t, but it is a consequence of the equations of motion (4.4),

and hence of (4.1), that *the eigenvalues* $\lambda_1,...,\lambda_N$ *of* L *are independent of* t [3]. The eigenvalues of L, therefore, are *constants of the motion* for the Toda chain. Observe that the quantities

$$I_k \equiv \text{Trace}(L^k) = \sum_{n=1}^{N} \lambda_m^k \qquad \text{for} \quad k = 1,..., N$$

are also constants of the motion; I_1 is proportional to the total momentum and I_2 is proportional to the total energy. The I_k are functionally independent and are in involution [15]. Therefore, as described in Section 3, the trajectory of each solution of the Toda chain (provided we ignore the center of mass motion) winds around some torus S in phase-space.

The key to the success of our method is the following fact. *The values of the action variables for the Toda chain are related to the shape of the graph of the characteristic polynomial of* L. Let us now explain the precise connection.

Imagine given initial conditions q_n^0, p_n^0. Construct L^0 from the corresponding a_n^0, b_n^0, and $L(t)$ from the solution $a_n(t)$, $b_n(t)$ of (4.4). The eigenvalues $\lambda_1,...,\lambda_N$ of $L(t)$ are independent of time and so equal the eigenvalues of L^0. From the characteristic polynomial of L,

$$\det(\lambda I - L) = \prod_{n=1}^{N} (\lambda - \lambda_n),$$

define a new polynomial $\Delta(\lambda)$, called the *discriminant of* L, by

$$\det(\lambda I - L) = \left[\prod_{n=1}^{N} a_n \right] [\Delta(\lambda) - 2].$$

Since

$$\prod_{N=1}^{N} a_n = \left(\frac{1}{2} \exp\left(-\frac{\beta\Gamma}{2} \right) \right)^N$$

and $\lambda_1,...,\lambda_N$ are independent of time, we conclude that the graph of Δ is also independent of time. The real reason for the introduction of $\Delta(\lambda)$ is found in the theory of difference operators with periodic coefficients. For the present exposition, a few comments must suffice. It turns out that $\det(\lambda I - 1)$ oscillates roughly between the values $-4\prod_{n=1}^{N} a_n$ and 0, often overshooting them but never failing at least to reach them. The introduction of $\Delta(\lambda)$ scales and symmetrizes the situation (and the choice of "-2" is convention only; any other fixed number would do as well). One can verify [15] that in the trivial case $a_n \equiv \frac{1}{2}$, $b_n \equiv 0$, corresponding to an initial condition in which the chain is at rest, $\Delta(\lambda)$ is a Chebyshev polynomial, assuming its extrema ± 2 as often as possible, i.e., $(\deg \Delta) - 1 = N - 1$ times. It then turns out that any change in a_n and/or b_n raises maxima about $+2$, or lowers minima below -2, or both. This experience shows that the roots of $\Delta(\lambda) = -2$ also carry information about

the entries of L, even though the actual eigenvalues of L are the roots of $\Delta(\lambda) = 2$. The following result describes the shape of Δ [9, 15–17]:

The Nth degree polynomial Δ always has $N-1$ real extrema, and at these extrema $|\Delta| \geqslant 2$. Consequently, the roots of $\Delta = 0$ are real and have multiplicity 1, *while the roots of $\Delta = \pm 2$ are real and have multiplicity* 1 *or* 2.

Starting from the right, as depicted in Fig. 2, denote the intervals in which $|\Delta(\lambda)| \geqslant 2$ by $[\Lambda_3, \Lambda_2]$, $[\Lambda_5, \Lambda_4]$, etc. These intervals, which may degenerate to a single point, are called *gaps*. If $\Lambda_{2j+1} \neq \Lambda_{2j}$ we say the jth gap is *open* or *nonzero*; otherwise we say the jth gap is *closed* or *zero*. The most basic information provided by Δ is the number and the arrangement of the open gaps, as we will see in Section 5. The size of Δ for λ in a gap will also be important; sometimes we refer to the part of Δ over a gap as a *bump*.

THEOREM [14–17]. *The number of degrees of freedom excited by an initial condition equals the number of open gaps in the graph of Δ. If there are $k \leqslant N-1$ open gaps, the solution trajectory lies on a k-dimensional torus. The value of jth action variable* (3.4) *is*

$$\frac{2}{\pi}\int_{\Lambda_{2j+1}}^{\Lambda_{2j}} \cosh^{-1}\left(\frac{|\Delta(\lambda)|}{2}\right) d\lambda.$$

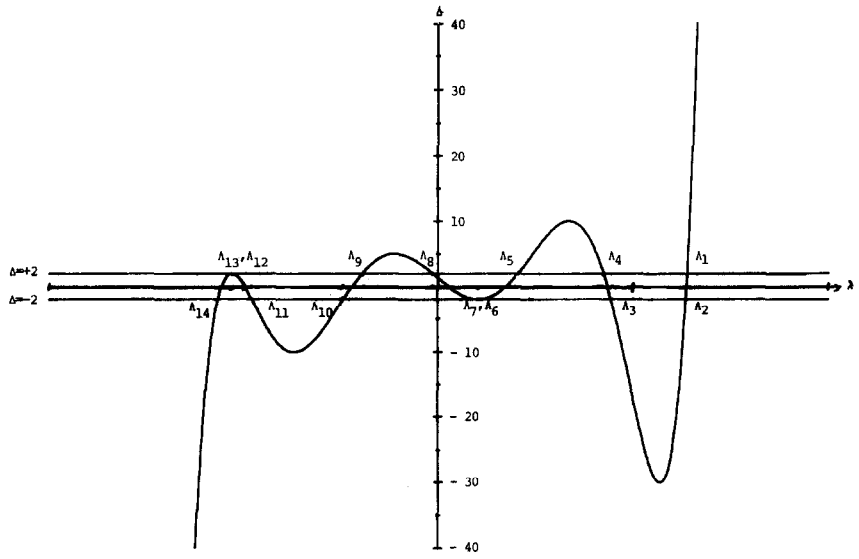

FIG. 2. A discriminant. The values of $|\Delta|$ at its extrema were prescribed (30, 10, 0, 5, 10, 0) and Δ was reconstructed by Kammerer's algorithm as described in [9].

Remark. This result is obtained as follows. One performs canonical transformations from q_n, p_n to conjugate variables defined via spectral properties of L. These are: $\mu_1,...,\mu_{N-1}$, the eigenvalues of the reduced matrix (A.5) in Appendix 2, and $f_1,...,f_{N-1}$, where $f_j = -2\cosh^{-1}(|\Delta(\mu_j)|/2)$. The loop integral (3.3) then reduces to

$$-\frac{1}{2\pi}\int f_j\, d\mu_j$$

taken around the loop from Λ_{2j} to Λ_{2j+1} and back, $\cosh^{-1}$ being given determinations of opposite sign on the "top" and "bottom" of the circuit. The detailed calculations are tedious, and the reader is referred to the original papers.

The procedure for getting a graphical display of the action variables corresponding to a given initial condition should now be fairly clear:

(1) Compute Δ from the characteristic polynomial of L^0 (there is a simple recursion relation which follows from the nearly tri-diagonal structure of L^0, see Appendix 2).

(2) Plot the graph of the *modified discriminant*:

$$m(\lambda) = \Delta(\lambda) \qquad \text{if} \quad |\Delta(\lambda)| \leqslant 2,$$

$$= \operatorname{sign}(\Delta(\lambda))\left\{2 + \frac{2}{\pi}\cosh^{-1}\left(\frac{|\Delta(\lambda)|}{2}\right)\right\} \qquad \text{if} \quad |\Delta(\lambda)| \geqslant 2.$$

The value of the action variable J_i will be the area under the ith bump of the graph of $m(\lambda)$.

To interpret the figures which follow, keep in mind that *we always plot* $m(\lambda)$; out of habit, and because the whole theory really revolves around Δ, we refer to the graphs as "discriminant plots."

We re-emphasize that the action variables will for us play the role of normal-mode amplitudes. We want to understand the relation between a given distribution of action variables (computed once and for all at the initial time) and the later motion of the Toda chain. In the next section, we investigate this correspondence by studying a variety of relatively simple examples.

5. Practice Problems

In this section, we take various initial conditions and plot the graph of m, as well as the graph of a_n versus t, for $n = 1,..., N$, (see (4.3).) In the process, we will discover various rules relating the action variables to the motion of the Toda chain. The information which can be extracted from a discriminant plot is of two types:

(1) Rigorously provable facts, and

(2) Rules of thumb which are deduced by extrapolation from computer experiments.

Recall the basic relation (stated in the Theorem at the end of Section 4) between the number of open gaps and the number of degrees of freedom. There are other rigorous facts, some of which might make matters clear for experts, we will simply try to make the various rules plausible with a series of graphs.

The best known solution of the periodic Toda chain is the traveling wave discovered by Toda [1]. It is expressed explicitly by elliptic functions. As limiting cases, it includes the sinusoidal normal modes of the harmonic chain, as well as the localized soliton solutions of the infinite Toda chain (see Appendix 1). We begin with these extreme cases.

EXAMPLE 1. *Harmonic Normal Modes.* The jth harmonic normal mode with amplitude a is (see (2.6))

$$q_n^{(j)} = \sqrt{\frac{2}{N}} \frac{a}{\omega_j} \sin(k_j n + \omega_j t), \tag{5.1}$$

where

$$k_j = \frac{2\pi j}{N}, \qquad \omega_j = 2 \sin(k_j/2).$$

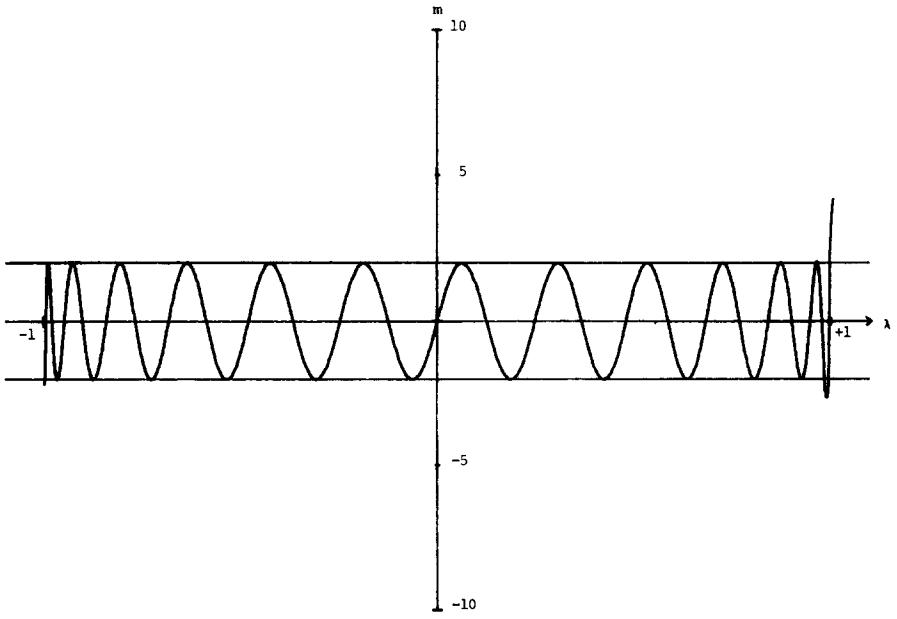

FIG. 3. Modified discriminant for harmonic normal mode 1, amplitude = 0.04. Note the very small second action.

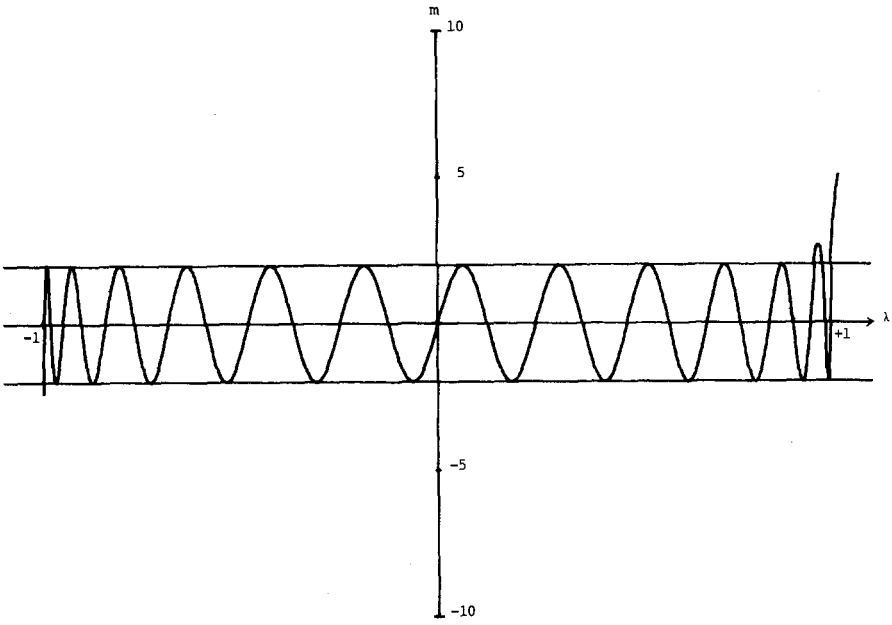

FIG. 4. Modified discriminant for harmonic normal mode 2, amplitude = 0.04.

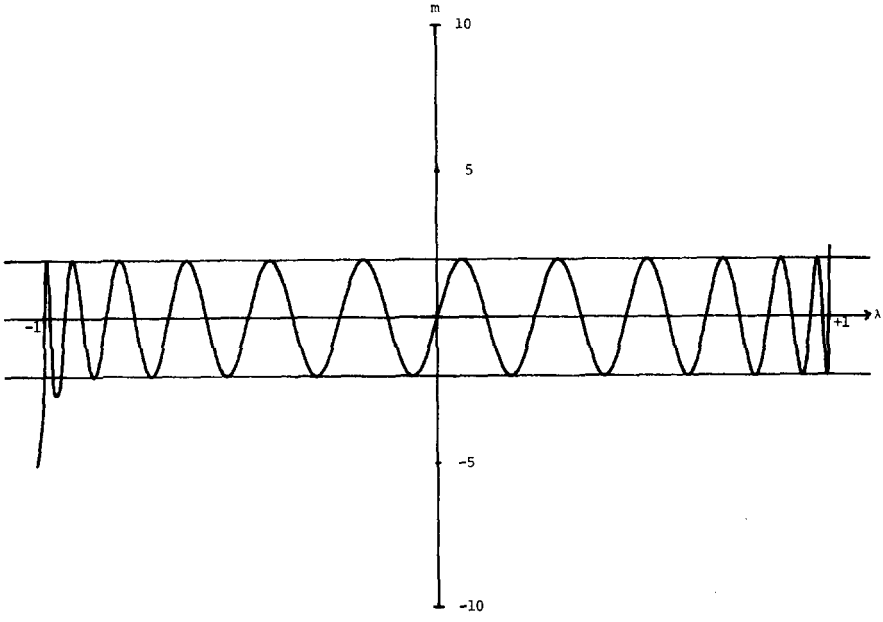

FIG. 5. Modified discriminant for harmonic normal mode 23, amplitude = 0.04.

This is only an approximate solution of the Toda chain, the approximation getting better as the amplitude $a \to 0$. Figures 3–5 show the discriminant computed from the initial conditions (5.1) for $j = 1, 2, 23$ for an $N = 25$ chain; $a = .04$.

To plotter accuracy, only one action variable is excited: all but one of the extrema of $|\Delta|$ equal 2; the excited action variables correspond, respectively, to extrema 1, 2, 23. One can *prove*, either from explicit formulas involving elliptic functions, or by perturbation about the state where $(q, p) = (0, 0)$, that with a small amplitude jth harmonic normal mode as an initial condition, the jth gap is opened much more than the other gaps. Thus we have:

RULE 1. *A small amplitude harmonic normal mode excites essentially only one Toda action variable. Mode j opens the jth gap (from the right). The open gap is located inside the interval* $-1 < \lambda < +1$.

Remark 1. Recall from Section 2 that the harmonic normal modes run to the left for $j = 1,..., N - [N + 2/2]$ and to the right for $j = [N + 2/2],..., N - 1$.

Remark 2. The fact that the open gap is inside $[-1, +1]$ is important. We will see shortly that gaps corresponding to solitons lie almost entirely outside $[-1, +1]$. We think of this distinction as a periodic analog of the inverse scattering characterization of solitons and ringing: solitons are characterized by the roots of Δ outside $[-1, +1]$ and ringing is characterized by the amplitude of Δ inside $[-1, +1]$ (see [3, 4, 18]). In the inverse scattering theory, "ringing" refers to all waves that are not solitons. For the infinite chain, these turn out to be the dispersive wavetrains familiar from the asymptotics of the harmonic chain, with some small-amplitude wavelength corrections due to the nonlinearity.

Remark 3. From the wavenumber formula $k_j = 2\pi j/N$, one sees that gaps near $\lambda = \pm 1$ correspond to long wavelength excitations, gaps near $\lambda = 0$ correspond to short wavelength ("optical") excitations. The center-of-mass motion (mode N) requires special consideration and will not be dealt with in this paper.

EXAMPLE 2. *One Soliton.* The *infinite* Toda chain supports localized traveling compressional waves (solitons), given explicitly by Toda's formula (for Γ in (4.1) equal to 0):

$$4a_{n-1}^2 - 1 = \sinh^2(\gamma)\,\operatorname{sech}^2(\gamma n \pm t \sinh(\gamma) + \delta). \tag{5.1}$$

If the speed and amplitude are large ($|\gamma|$ large) the wave is concentrated on just a few masses (see Fig. 6 for a picture of this kind of solution). Formula (5.1), taken only for $n = 1,..., N$, is not an exact solution of the equations of motion for the periodic chain. There are, however, exact solutions which are periodic superpositions of solitons (5.1):

$$4a_{n-1}^2 - 1 = \sum_{k=-\infty}^{\infty} \beta^2 \operatorname{sech}^2\{\alpha(\gamma - \mu k) - \beta t\} - 2\beta v \tag{5.2}$$

(see [1e] and Appendix 1). In the limit as $\mu \to \infty$ the parameter $\beta \to \sinh(\gamma)$ and so (5.2) can be considered to be a periodic superposition of (distorted) solitons which are described by (5.1). The fact that in general $\sinh(\gamma) \neq \beta$ can be viewed as compensating for the interaction between the exponentially small tails of the superimposed soliton shapes. In our experiments, we have found that a profile generated by (5.1) with $|\sinh(\gamma)| = 1.1$ in an $N = 10$ chain is so localized that (to plotter accuracy) there is no difference between the single sech-squared profile (5.1) and the exact formula (5.2) with $\mu = 10$.

In the rest of the paper, when we speak of "solitons in the periodic Toda chain," we are being deliberately imprecise: we will have in mind either the exact solution (5.2) which looks like, but is not, a superposition of solitons (5.1), or a truncated soliton (5.1) which is not an exact traveling wave solution. The difference cannot be seen on our plots.

Now to the graph of Δ, computed from an initial condition (5.1) with the speed $\sinh(\gamma)/\gamma = 1.5$ and $N = 25$. In Fig. 6 we present the timeline plot of a_n for $n = 1,\ldots, N$ and $0 < t < 50$; this plot shows a typical soliton shape. In the graph (Fig. 7) of the (modified) discriminant recall that the vertical scale is linear when $-2 < \Delta < +2$ and logarithmic when $|\Delta| > 2$. This accounts for the nonpolynomial shape of parts of all graphs of the discriminant. The value of the discriminant at its maximum ($\sim 10^{15}$) is entirely typical, and perhaps surprisingly large for someone who has done inverse

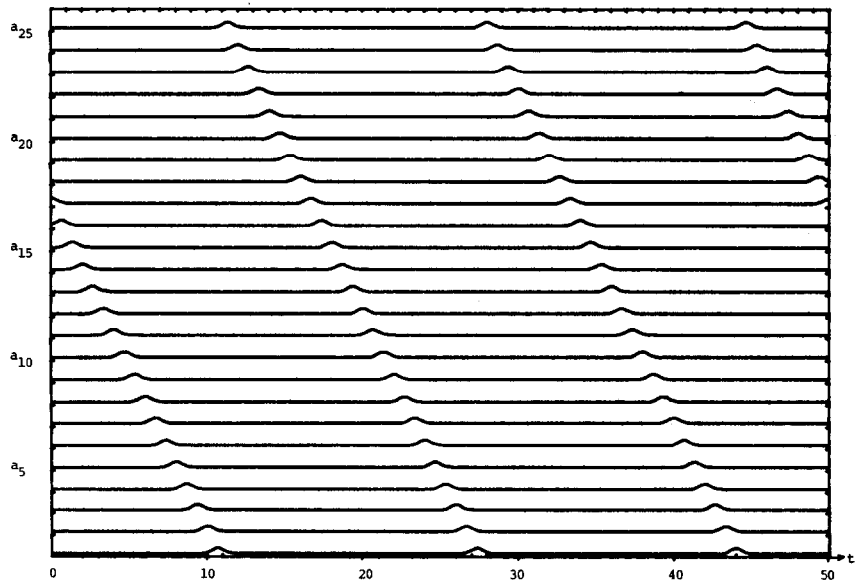

FIG. 6. Plot of a_n versus t for $1 \leqslant n \leqslant 25$, one infinite-chain soliton speed 1.5 placed in an $N = 25$ periodic chain. The bottom curve is a_1.

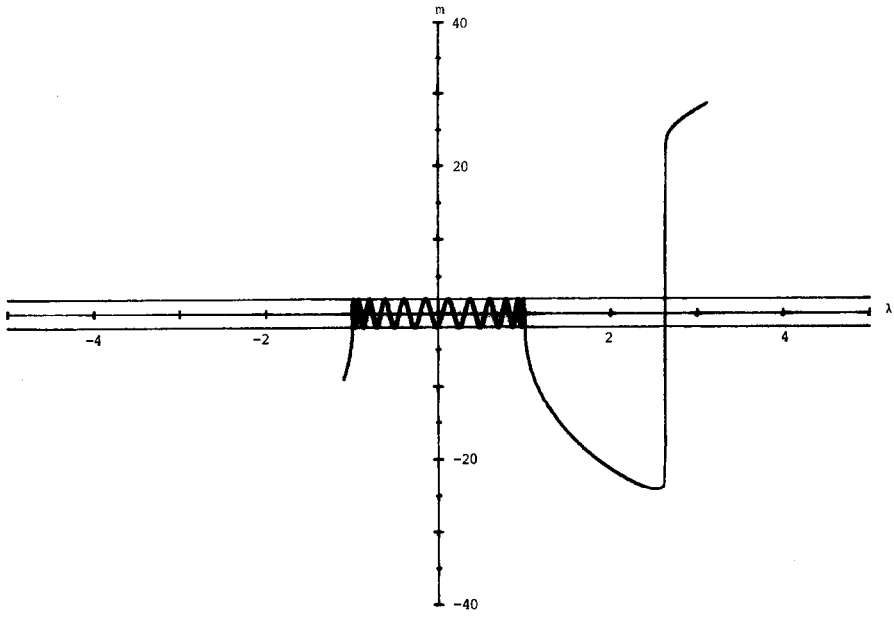

FIG. 7. Modified discriminant for Fig. 6.

spectral theory with pencil and paper only. The discriminant plot of Fig. 7 suggests the next rule:

RULE 2. *A single localized soliton in a periodic Toda chain corresponds to a single excited action variable. The one open gap lies outside* $-1 < \lambda < +1$; *it is the leftmost (or rightmost) gap of* Δ *if the soliton travels to the right (or left).*

Remark 4. Again, one can *prove* that an exact traveling wave solution (5.2) leads to a discriminant with just one bump. We cannot prove that this gap lies outside $[-1, +1]$; this is an asymptotic result. "Asymptotic" means: the result becomes exact as the soliton amplitude tends to ∞.

Remark 5. If only one action variable is nonzero, the solution trajectory lies on a one-dimensional torus, i.e., a closed curve, in phase space. Hence it is necessarily time-periodic.

Remark 6. The exact value of the nonzero action variable is (for a left-running soliton)

$$J_1 = \frac{2}{\pi}\int_{\Lambda_3}^{\Lambda_2} \cosh^{-1}\left(\frac{|\Delta(\lambda)|}{2}\right) d\lambda$$

according to the theory summarized in Section 4. Integration by parts yields

$$J_1 = -\frac{1}{\pi}\int_{\Lambda_3}^{\Lambda_2} \frac{\lambda\, d\lambda}{\sqrt{\Delta^2(\lambda)-4}}. \tag{5.3}$$

Since Λ_2 is a simple root of $\Delta^2 - 4$, the integral converges. Note how steep Δ is at Λ_2: typically $|(\Delta - 4)/\Delta'| < 10^{-7}$. So from the standpoint of computation, the integral (5.3) would be singular if we used only seven decimal places of accuracy in the computation of the Λ_i's. This makes the numerical evaluation of (5.3) quite delicate. Similar integrals occur in formulas for the frequencies $\partial H/\partial J_i$ associated with the action variables, and in the definition of the θ-functions which provide the exact solutions to the Toda equations [15, 16]. This is one reason why the exact formulas seem to be of little practical use.

There is one more important item which can be read from the graph of Δ: *the soliton speed.* Let λ be the zero of Δ between Λ_1 and Λ_2.

RULE 3. *The soliton speed is given by*

$$\frac{\sqrt{\lambda^2-1}}{\ln(|\lambda| + \sqrt{\lambda^2-1})}. \tag{5.4}$$

(This is an asymptotic result ("asymptotic" as explained in Remark 4); see [18] for a heuristic explanation of (5.4) using the infinite-chain inverse scattering theory.)

Remark 7. The bigger the bump, the larger and faster the soliton. One precise measure of this relation can be derived for the one-soliton solution: Amplitude of p_n = two times the width of the gap.

EXAMPLE 3. *One nonzero action variable.* If only one action variable is different from zero, the solution lies on a one-dimension torus in phase space, and so must be time-periodic. We have already seen two illustrations. If the jth action variable is only slightly different from zero (all others being zero), the motion is approximately the jth linear normal mode. If the first or last action variable is large (all others zero) and outside $-1 < \lambda < +1$, the solution is a soliton well localized in the chain. In general, if the jth action variable is the only nonzero action variable then the solution is a traveling wave described by (5.2) with $\mu = \max\{N/j, N/N-j\}$. Such a solution has N/μ spatial periods in the N-particle chain. If γ (and hence β, see Appendix 1) is small, this is the jth linear mode. If γ is large, the sech-squared profiles in (5.2) overlap little, and the solution appears as a sequence of N/μ equally spaced solitons, all with the same speed. For intermediate γ, the solution is a wave of period N/μ, too large to be a linear mode but not localized enough to be considered a soliton.

An example is shown in the discriminant plot of Fig. 8. Gap 4 of seven gaps is open; the spatial period of the excitation is 2. The timeline plot (Fig. 9) shows this to be a sort of optical mode [19, p. 78 ff.]; the springs are alternately stretched and compressed, and the wave does not propagate.

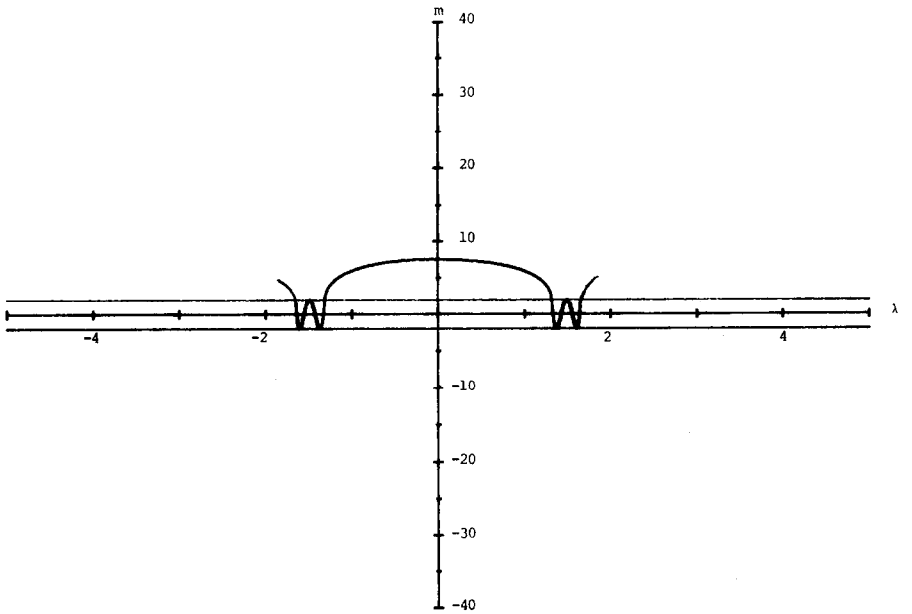

FIG. 8. Modified discriminant for Toda's standing wave (wavelength 2) in an $N = 8$ chain; $q = 0.25$ in formula (A.2′), Appendix 1.

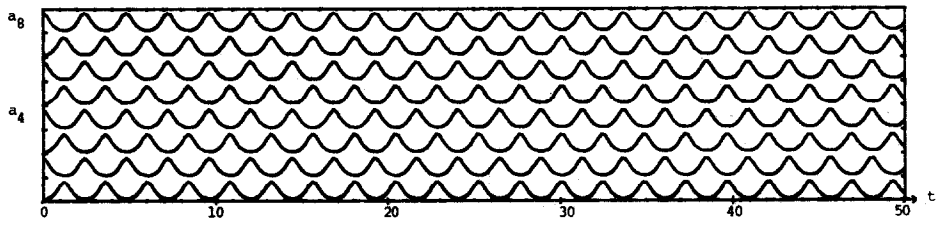

FIG. 9. a_n versus t plot for Fig. 8.

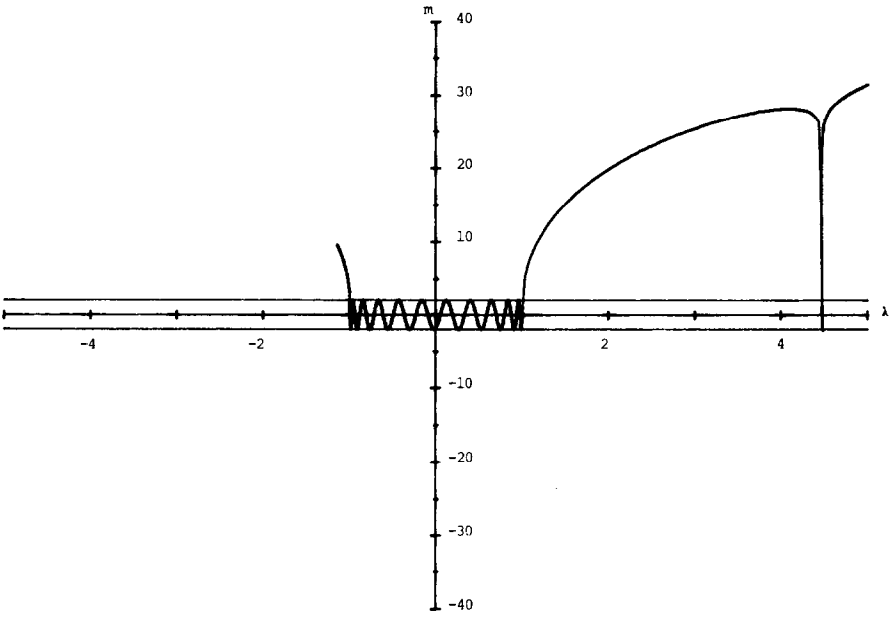

FIG. 10. Modified discriminant for two speed 2 solitons equally spaced in an $N = 24$ chain.

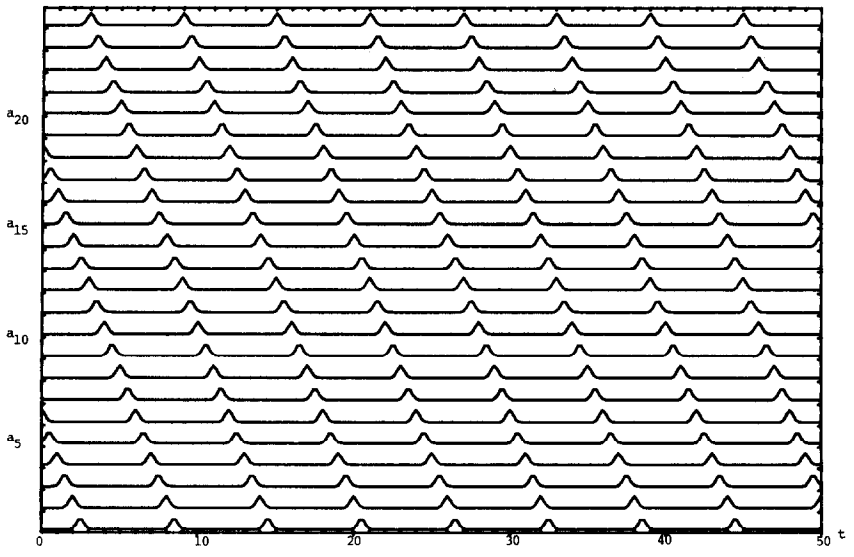

FIG. 11. a_n versus t plot for Fig. 10.

Note that the gap is neither inside nor outside $[-1, +1]$, and it is indeed not possible to think of the solution as linear or soliton-like. There are, however, solitons "hidden" in the wave: we return to this in Example 5, after we have discussed discriminants of multi-soliton solutions.

A soliton-like excitation is associated with the discriminant of Fig. 10. Note that the gap is entirely outside $[-1, +1]$. The solution is near the soliton limit of (5.2), and the timeline plot (Fig. 11) shows two localized soliton shapes of equal speed.

EXAMPLE 4. *Two Solitons.* How is the presence of two soliton-like pulses reflected in the action variables? First, we describe the discriminant plots very briefly; then we summarize the rules to be learned from these graphs.

Case 1. A soliton (5.1) of speed 1.5 is centered on mass 17 and a soliton of speed 2 is centered on mass 5 in an $N = 25$ chain; the solitons are traveling in opposite directions. The timeline picture (Fig. 13) is a familiar one. On the plot of the discriminant (Fig. 12) there are two nonzero action variables. The larger one on the right corresponds to the faster, *left-running* soliton.

Case 2. The solitons are centered as in Case 1 except the solitons are now traveling in the same direction (Fig. 15). Again the discriminant plot (Fig. 14) shows two nonzero action variables. This time the corresponding gaps are both on the *right*, indicating that both solitons run to the *left*.

Case 3. If we take two solitons (5.1) of *equal* speeds, centered on masses 6 and 18 of an $N = 24$ chain, there is only one action variable excited. This is the case discussed in Example 3, Figs. 10 and 11. If the symmetrical placement of these solitons is disturbed, more than one action variable is excited.

Case 4. The solitons are centered as in Case 3 but now their speeds are 2 and 1.9. Note in Fig. 16 that action 2 still dominates; the now present action 1 is fairly small. This might be expected, if one considers the change in speed from 2 to 1.9 to be a small perturbation of the data in Case 3: newly excited action variables should remain small.

Case 5. We perturb the configuration of Case 3 by placing two solitons (5.1), both of speed 2, unsymmetrically into an $N = 24$ chain. The timeline plot (Fig. 17) seems to indicate that these solitons propagate through the chain at their original separations. We know, however, that the periodic Toda chain does not have a traveling-wave solution composed of two unequally spaced peaks, and indeed the discriminant plot (Fig. 18) shows an extremely small but nonzero value for action variable J_1. We surmise that our initial condition consists of two solitons of almost equal speeds (a difference of 10^{-2} is an overestimate), plus a small contribution from other action variables. The latter are not visible in Fig. 18, but their effect at $t = 0$ would be to increase the size of one soliton slightly so that the two initial peaks appear to be identical. After a long time, we expect the solitons to have separated enough to be symmetrically spaced in the chain. Hence the present case is the same as Case 4, with a much smaller speed difference.

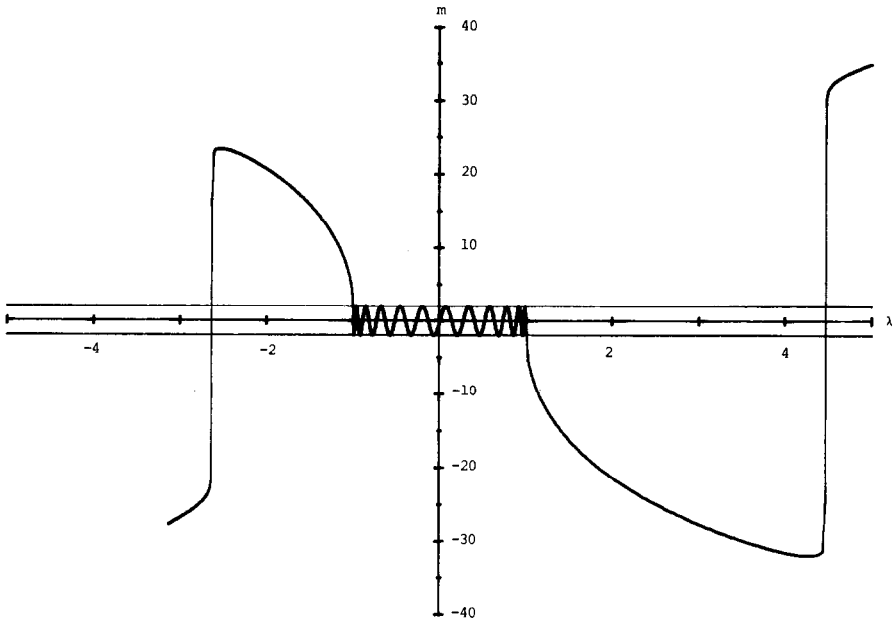

FIG. 12. Modified discriminant for two colliding solitons (Example 4(i)).

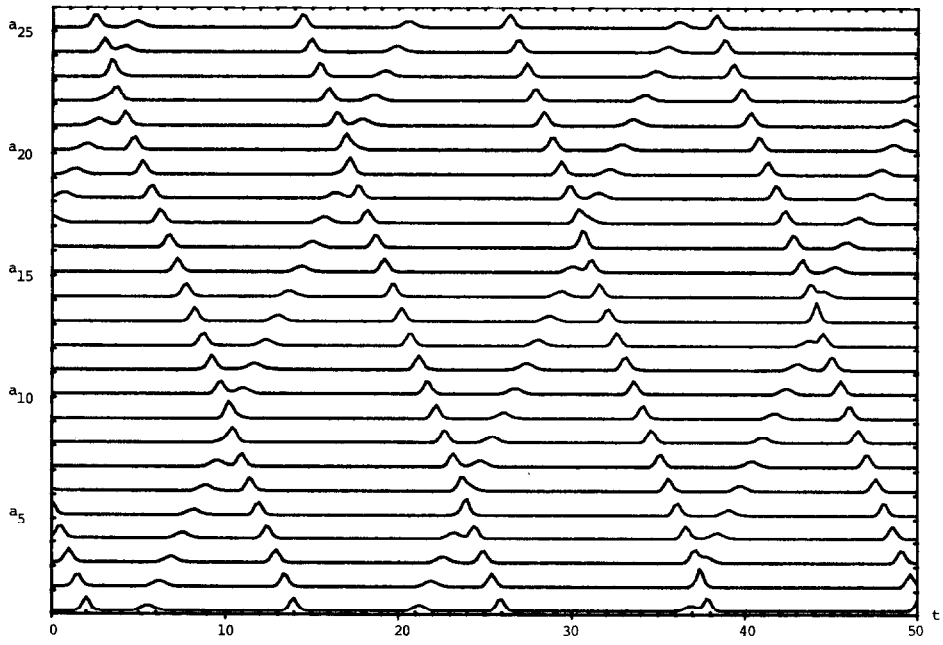

FIG. 13. a_n versus t plot for Fig. 12.

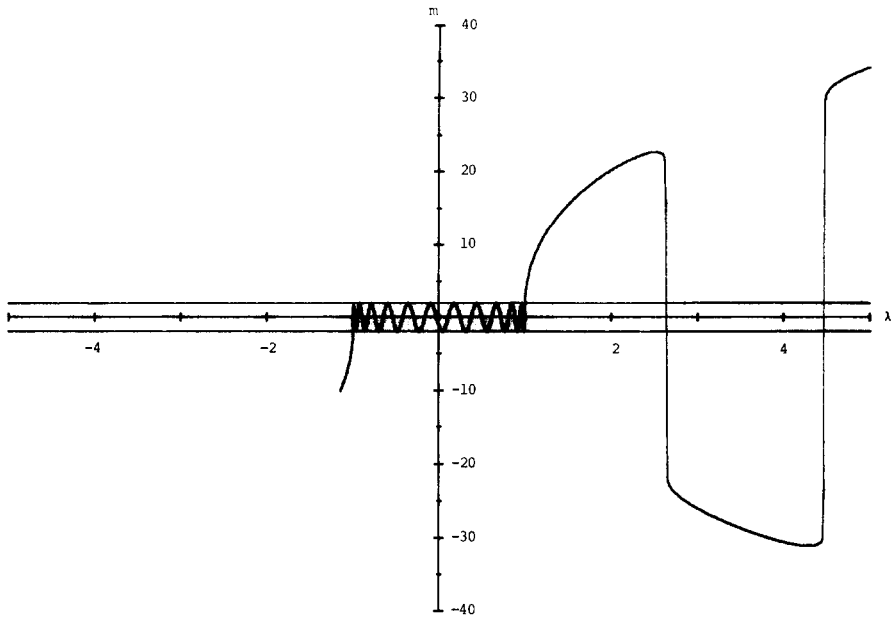

FIG. 14. Modified discriminant for two solitons running in the same direction (Example 4(ii)).

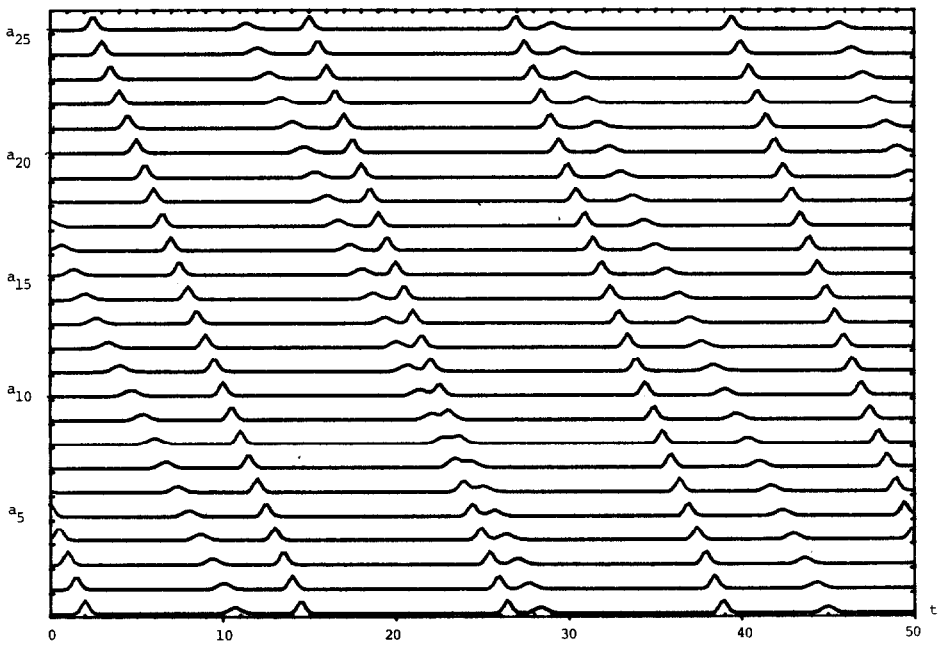

FIG. 15. a_n versus t plot for Fig. 14.

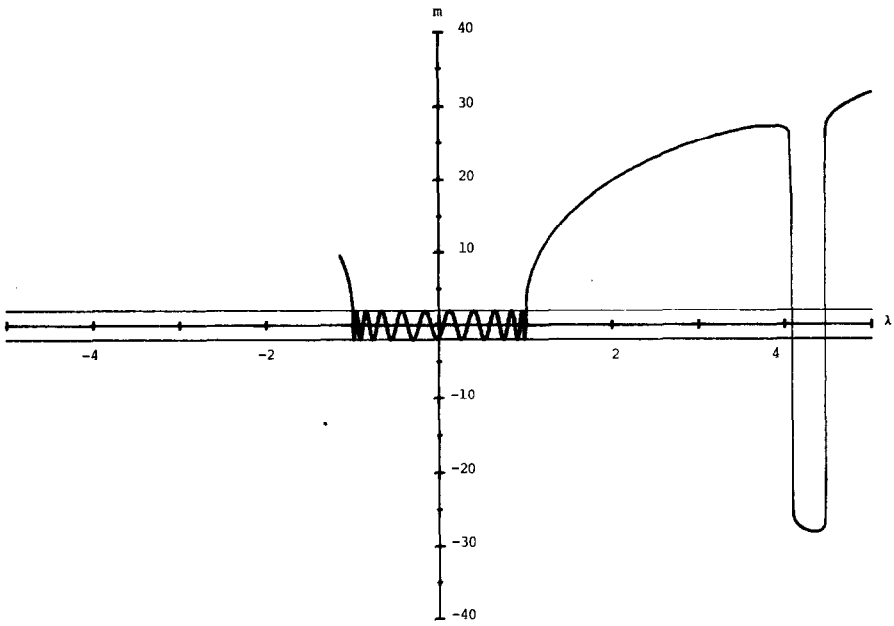

FIG. 16. Modified discriminant for solitons of slightly different speeds (Example 4(iv)).

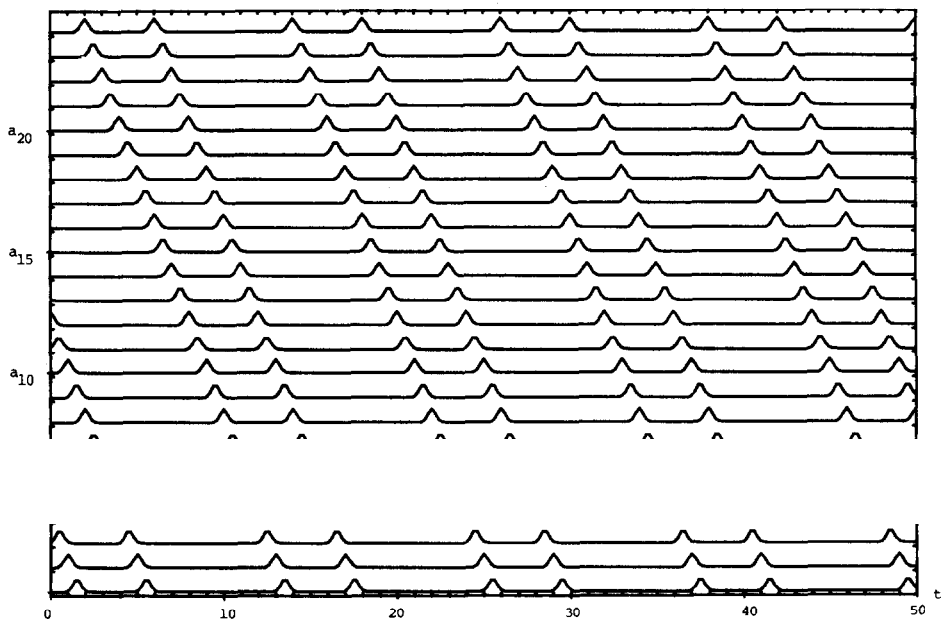

FIG. 17. a_n versus t for two infinite-chain, speed 2 solitons placed unsymmetrically into an $N = 24$ chain. (Example 4(v)).

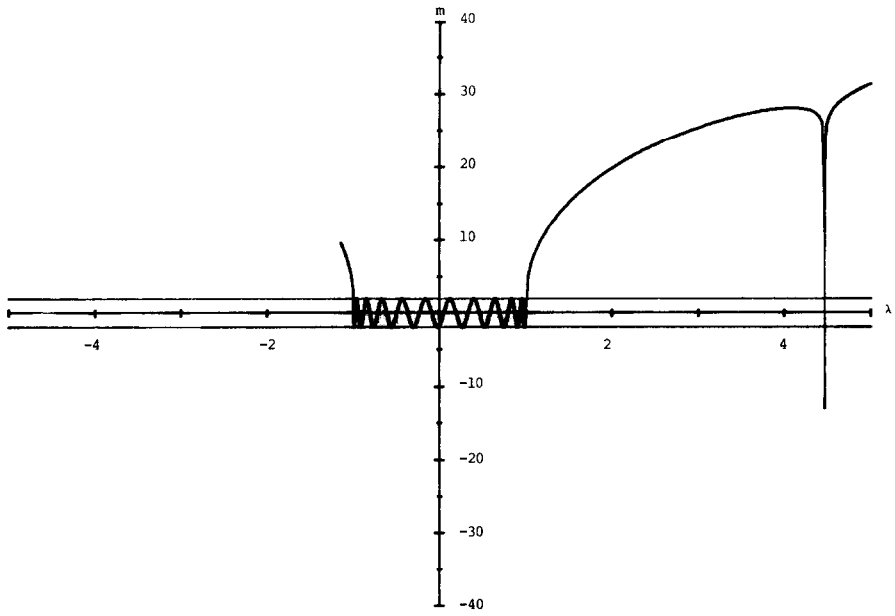

FIG. 18. Modified discriminant for Fig. 17.

The plots above show the possibilities for the action variables corresponding to two solitons to be quite varied and, to our mind, surprisingly subtle. Let us now summarize what can be learned from these examples.

First, we restate for emphasis: *action variables arising from gaps outside* $-1 < \lambda < +1$ *indicate the presence of soliton-like waves.* "Soliton-like" is intended to underscore that these are solutions of the periodic chain which look like solitons; they are *not* the exact solitons of the infinite chain.

Next, we want to predict the number of solitons.

RULE 4. *If the kth gap (from the right) is the last nonzero gap to the right of* $\lambda = 1$, *there are altogether k left-running solitons. (Likewise for gaps to the left of* $\lambda = -1$.)

The solitons may be of greatly different speeds, they may have equal speeds, or they may fall into groups, the speeds within each group being equal, or nearly equal, etc. There are correspondingly many possibilities for the sizes of the k action variables in $|\lambda| > 1$. For us, two extreme cases will be most important:

RULE 4a. *All k action variables to the right of* $\lambda = +1$ *(or the left of* $\lambda = -1$*) are nonzero. In that case, there are k solitons of different speeds.*

RULE 4b. *Only the kth action variable is nonzero. Then the solution is a traveling wave made up of k equally spaced solitons traveling at equal speeds (see Example 3).*

Other cases can be deciphered, if they are simple enough, by analogy with Cases 1–5 above. Suppose, for example, that the fifth action is large, the second is small, and all others are zero. We expect (cf. Case 5) to find five solitons, three of one speed and two of a different speed.

The *rule for computing soliton speeds* remains the same as for the single-soliton case. The predicted speed of the soliton, or group of solitons, associated with the jth gap is

$$S^* = \frac{\sqrt{\lambda^2 - 1}}{\ln(|\lambda| + \sqrt{\lambda^2 - 1})},$$

where λ is the root of the discriminant at the outside edge of the jth gap ("outside" means in the direction of increasing $|\lambda|$). Note on the plots of the discriminant in the present example that the discriminant is extremely steep at these roots; the relative error $|(S - S^*)/S|$, S being the true speed, will be small as long as the discriminant is steep and the roots are not too close to $\lambda = +1$. We should point out that the "true" speed of a soliton is usually estimated from a timeline plot or a printout, and so the concept of soliton speed is intrinsically not very accurate for the periodic chain.

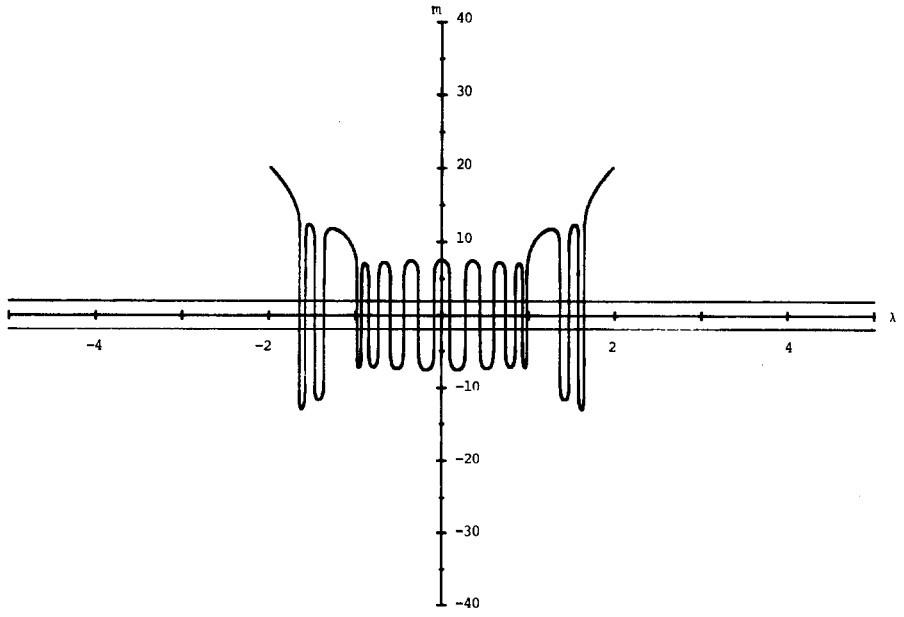

FIG. 19. Modified discriminant for Example 5.

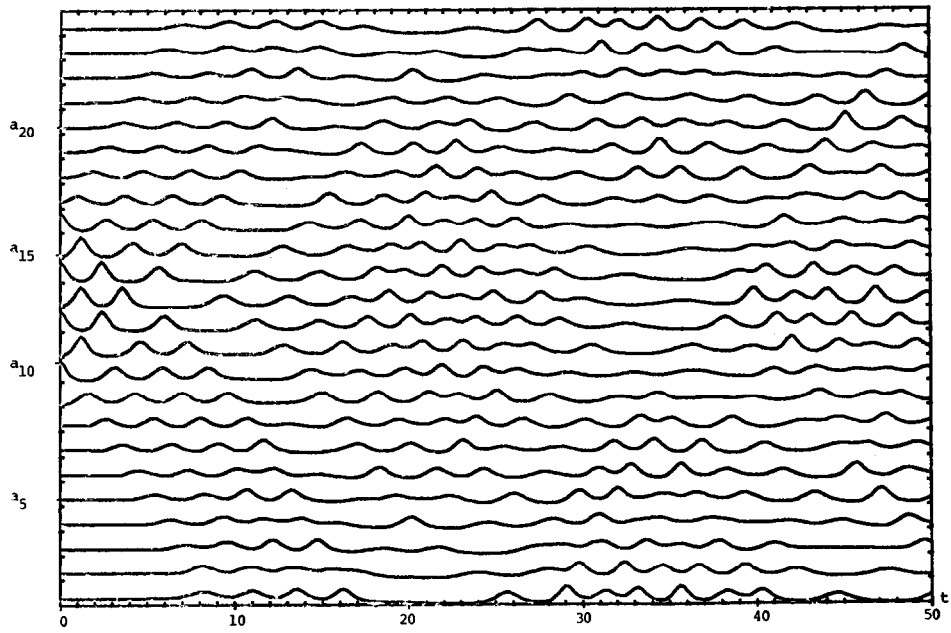

FIG. 20. a_n versus t plot for Fig. 19.

EXAMPLE 5. *Many solitons.* In Example 3, we looked at a gap 4 excitation on an $N = 8$ chain (see Figs. 8 and 9). We pointed out that it is not possible to identify solitons in the solution. Even though (5.2) exhibits the standing "optical" wave as a

to be distinguishable. We can, however, give them time to separate, by adding masses *at rest* on both sides of the original $N = 8$ initial condition. We have added eight masses on each side in this computation.

The change in the discriminant is dramatic (Fig. 19). All 23 action variables are excited. Note, first of all, four soliton actions on the outside of $|\lambda| = 1$. The fourth action from each end is significantly larger than the others. The fourth actions alone would correspond to trains of four soliton shapes equally spaced and of equal speeds (four moving right and four moving left). The smaller values of the three outermost actions on each side signify a perturbation rendering the four speeds slightly unequal (one can distinguish these on Fig. 20). The large action variables inside $-1 < \lambda < +1$ probably provide interference from *all* possible Toda modes in order to produce the 16 masses initially at rest. The flavor of this last statement is strikingly linear in its appeal to interference of normal modes, even though the "superposition" of these normal modes is decidedly nonlinear. Our guess is based on experience only; there is no supporting theory. Compare Example 7 for another appeal to superposition of modes.

EXAMPLE 6. *A sine wave.* The initial condition on an $N = 25$ chain is a *large* amplitude harmonic mode 1 (amplitude 1),

$$q_n = \sqrt{\frac{2}{N}} \frac{1}{\omega_1} \sin(k_1 n + \omega_1 t).$$

There are only four action variables of any size, two corresponding to gaps outside $[-1, +1]$ and two to inside gaps (Fig. 21). The timeline plot (Fig. 22) shows four propagating pulses. We measured their speeds (with a ruler) at the right side of this plot, where the pulses are most separated and presumably experience the least interaction with each other. Repeated measurements produced the values: 1.06, 1.04, 0.99, 0.85. A 1/32″ difference in measurement can produce a 5% change in speed, so these are only crude estimates. Still, it is clear that two pulses are supersonic (speed > 1) and two are subsonic (speed < 1), conforming with the distribution of open gaps in Fig. 21. The soliton speeds computed from the roots of the discriminant at the outside edges of the gaps (cf. (5.4)) are 1.06 and 1.025; this is about as good an agreement as we have come to expect for such slow solitons. Now we look at the interior gaps. We surmise from Figs. 3, 4, and 5 (Example 1) that the small fourth

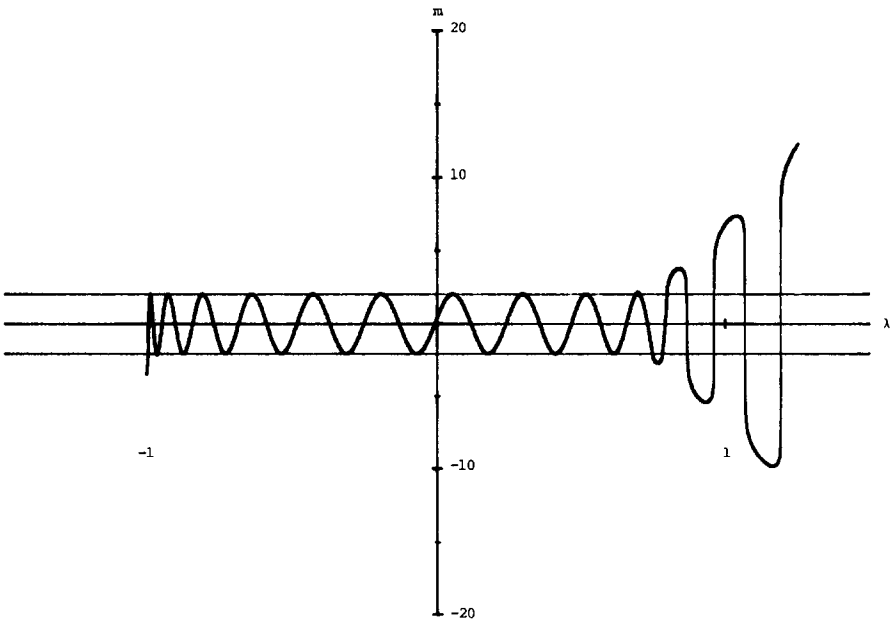

FIG. 21. Modified discriminant for amplitude 1 harmonic normal mode 1 on an $N = 25$ chain (Example 6).

action variable is a near linear Fourier mode with wavenumber $k_4 = 8\pi/25$. It comes from only the second gap inside $[-1, +1]$, and so one might guess that it corresponds to wavenumber k_2. Superposition of Figs. 3 and 21 shows, however, that the fourth extremum of the discriminant falls in almost the same place. The correct interpretation seems to be that gaps 1 and 2, and to some extent 3, have moved outwards from their natural closed position (Fig. 3). The small fourth pulse visible on Fig. 22 appears to be localized, and is therefore more likely to be group packet than a wavetrain. Indeed, the group velocity

$$\cos\left(\frac{k_4}{2}\right) = 0.88$$

is very close to the measured velocity of the pulse. (We do not really understand the interference mechanism which produces group packets; presumably it is a combination of solitons and of the very small, near linear actions, which cannot be seen on the discriminant plot.) The velocity of the third pulse in Fig. 22 is not so well predicted by the linear theory: $\cos(k_3/2) = 0.93$. The third action variable is quite a bit larger than the near-linear ones of Example 1; note that the discriminant is beginning to develop the asymmetric bump characteristic of soliton actions. We deduce from this example of rule of thumb:

RULE 5. *A small action variable corresponding to a gap inside* $[-1, +1]$, *will*

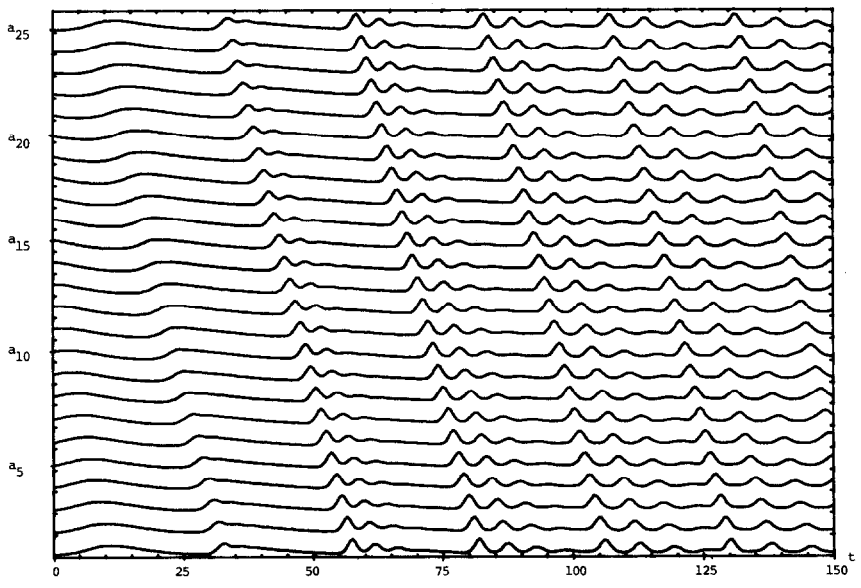

FIG. 22. a_n versus t plot for Fig. 21.

produce a near-linear group packet. The jth action gives a packet with approximate speed

$$\left|\cos\left(\frac{k_j}{2}\right)\right|.$$

EXAMPLE 7. *Impulse initial condition.* The initial condition has $q_{13} = 0, p_{13} = -6$ and $q_n = p_n = 0$ for all $n \neq 13$. From the discriminant plot (Fig. 23) we would predict one left-moving soliton with speed 1.61 determined from the first root of the discriminant, $\lambda = 3.34$. This soliton, of measured speed 1.6, can be seen on the timeline plot, Fig. 24. There are also some shapeless ripples, representing the cumulative effect of the action variables inside $[-1, +1]$. The interior actions are quite small, comparable in size to those of the near-linear modes of Example 1 (Figs. 3, 4 and 5). In view of Example 6, we would expect the ripples to be essentially linear wave packets moving with a group velocity $\cos(k/2)$. Their speed is evidently less than 1. Since *all* gaps are open in this case, we do not know how to predict from the graph of the discriminant which near-linear actions will cause the visible waves in the lattice. The matter could perhaps be resolved by computation of the values of all 24 action variables, but we have not done this.

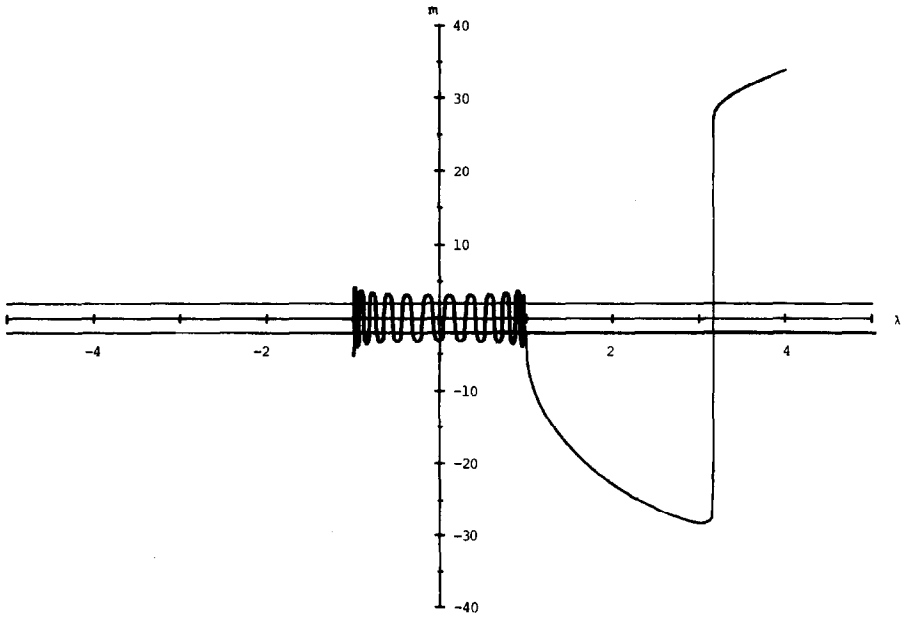

FIG. 23. Modified discriminant for impulse initial condition (Example 7).

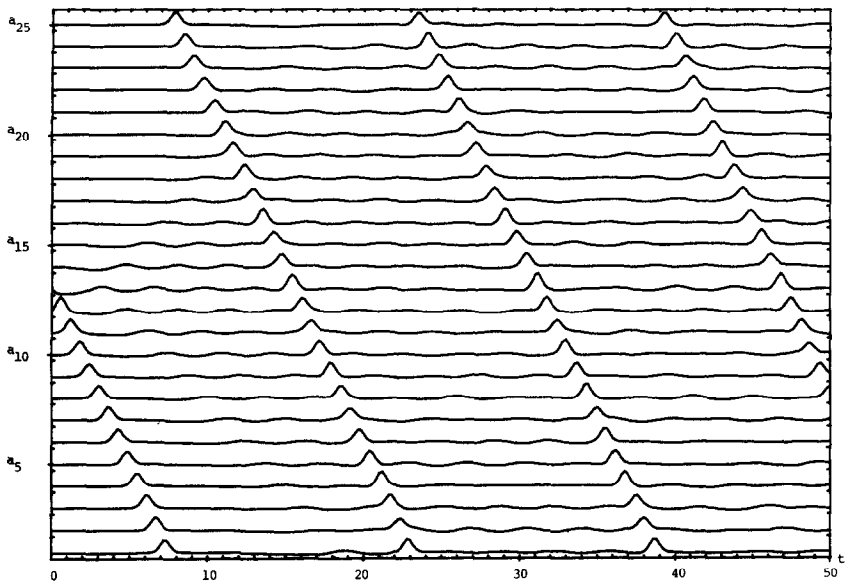

FIG. 24. a_n versus t plot for Fig. 23.

Let us now reflect on what our practice problems have taught us. The first point is that the knowledge of the action variables of the Toda chain can give information about the physical appearance of the chain. The state at a given time cannot be deduced, of course, because the angle variables are not specified, so that the relative phases of solitons, etc., are unknown. We can, however, draw some conclusions from the discriminant about the types of waves that will emerge *in the course of the motion.* As we said in the introduction, the Toda chain is the only nonlinear example known to us for which the mathematically pleasant action variables can be correlated with the physical motion.

The second important point is that the *sizes* of the action variables are not enough to describe the solution. It is necessary to know also *where they are located on the graph of the discriminant.* Compare, for example, the optical mode of Figs. 8 and 9 with a case in which the fourth gap lies more nearly outside $[-1, +1]$ (Fig. 19). Or compare Figs. 3 and 18: in the first, action 1 is small and nearly linear. In the second, action 1 is also rather small, but it signifies a slight perturbation of one of two equal-speed solitons. *The relative sizes of the action variables are as important as their individual sizes*, and this is a significant change from the situation familiar in the harmonic chain.

The third point to make concerns the applicability of the discriminant method. The most clear-cut statements can be made when the solution consists of solitons and near-linear waves. We have found the interpretation of the discriminant to be generally *easy* for localized initial data. When the initial data have compact support, the periodic Toda chain can be understood by the intuitively appealing inverse

scattering method, with its simple distinction between solitons and ringing. We will see in the next section that the discriminant's use is not limited to such situations. We can also analyze motions which evolve from nonlocalized initial disturbances, but we cannot always tell in advance whether a given initial condition will lead to an understandable discriminant. The scope of our method is perhaps best described as follows: *if the discriminant shows at most one or two large action variables inside* $[-1, +1]$, *the general features of the motion can be predicted qualitatively, and often quantitatively.* With several large interior action variables, the nonlinear superposition becomes too complicated to be covered by just a few rules.

6. Weakly Nonlinear Chains

Physicists often use a simplified model to analyze the motion of a more complicated system. In this section we will demonstrate that the Toda chain can be used as a simplified model of a class of weakly nonlinear chains.

Let us begin by considering one of the computational experiments performed by Fermi, Pasta and Ulam [10]. In this experiment they followed the time evolution of a 32-mass fixed-end chain (2.1–2.2) governed by the quadratic force law

$$F_Q(x) = -x - \tfrac{1}{4}x^2. \tag{6.1}$$

Starting from the initial condition

$$q_n = \sin(\pi n/33), \qquad q_n' = 0 \qquad \text{for} \quad n = 1,..., 32,$$

they had hoped to observe by computation how the chain would approach its "thermalized" state, a state in which the chain's energy is equally shared among its various degrees of freedom (see [19] for a discussion of this circle of ideas).

To use the discriminant to understand this experiment, we must first recall that discriminant analysis applies rigorously only to the periodic Toda chain. Thus we must replace the fixed-end conditions of this quadratic chain by equivalent periodic boudary conditions, and adjust the parameter β in the Toda force law (4.2) so that the first three terms in the McLaurin series of the Toda force law agree with (6.1). Therefore we consider the time evolution of a 66-mass periodic chain (2.1–2.3), governed by the same quadratic force law, starting from the initial condition

$$q_n = \sin(\pi n/33), \qquad q_n' = 0 \qquad \text{for} \quad n = 1,..., 66,$$

and compare it with the time evolution of the 66-mass periodic Toda chain (4.1, 4.2) with $\beta = -1/2$.

We integrated the equations of motion for the 66-mass periodic quadratic chain. Following Fermi, Pasta and Ulam we present in Fig. 25 a plot of the energy

$$E_k = |A_k|^2 + |A_{66-k}|^2$$

(see Section 2) contained in the Fourier modes with spatial period $66/k$ for $k = 1,..., 6$. At first, we see the expected flow of energy from long wavelength to short wavelength Fourier modes. After $t = 5{,}000$ seconds, however, this energy flow reverses itself until at $t = 10{,}000$ seconds the energy is essentially distributed among the Fourier modes as it was initially.

Next, we integrated the equations of motion for the 66-mass periodic Toda chain. We present in Fig. 26 a plot of the same energies E_k; observe that at no time do these energies differ by more than a few percent from the corresponding energies computed from the quadratic chain. Furthermore, the time when the initial energy distribution recurs is essentially the same for the two chains.

From these graphs it would appear that the results obtained by Fermi, Pasta and Ulam for this experiment can be explained in terms of the properties of the Toda chain. To strengthen this argument we present in Figs. 27 to 30 plots of the modified discriminant, evaluated at the indicated times. We construct the discriminant from $(q(t), p(t))$ *as though we were dealing with the Toda chain*; the motion, however, is governed by the quadratic force law. Note that the Toda action variables (the areas under the bumps in these plots) are nearly constant; this should be compared with the large variation of the energies E_k, numbers which are proportional to the action variables of the harmonic chain. Note that very few Toda actions are excited; those

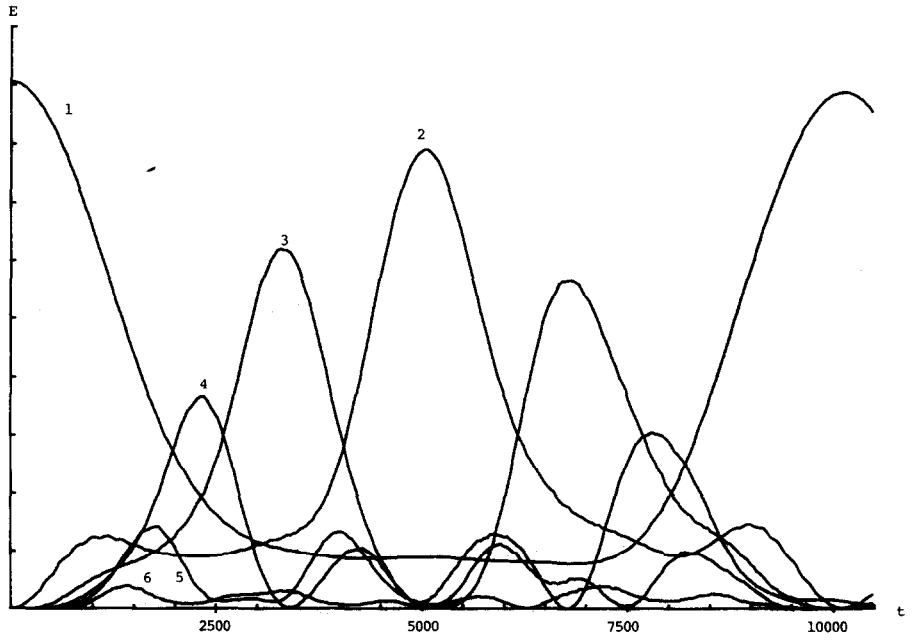

FIG. 25. Normal-mode energies as function of time for FPU experiment (data given in Section 6). Time scale: 500 per tic. Energy scale: 0.0005 per tic.

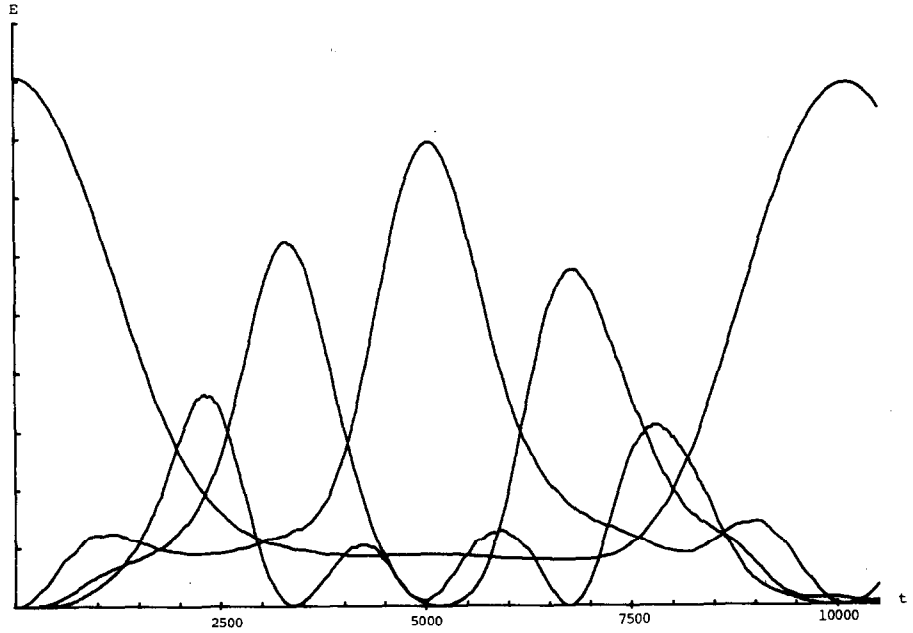

FIG. 26. The initial condition of Fig. 25 run for the Toda chain: plot of harmonic normal mode amplitudes. Superposition of Figs. 25 and 26 shows a shift, near the right side, of about one line's thickness.

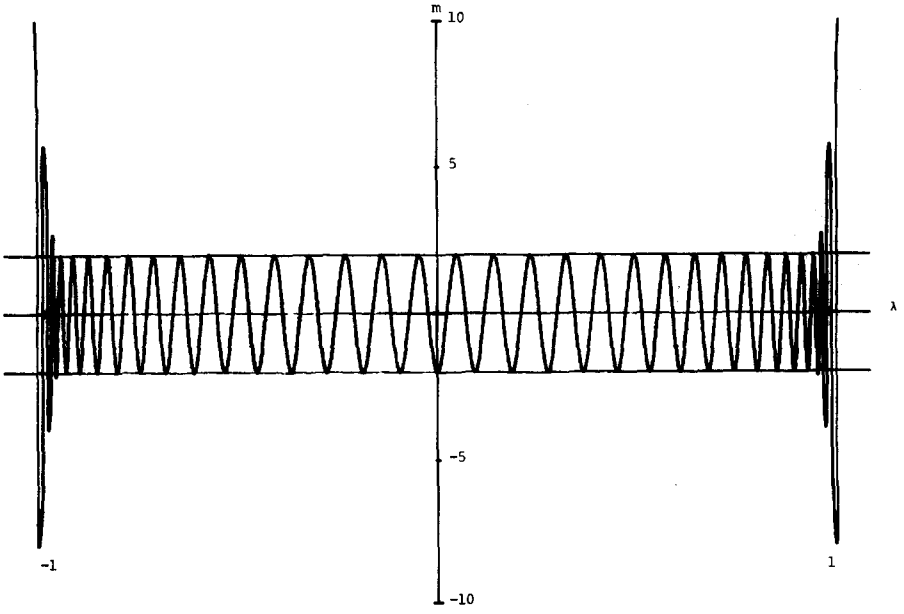

FIG. 27. Modified *Toda* discriminant for the FPU initial condition.

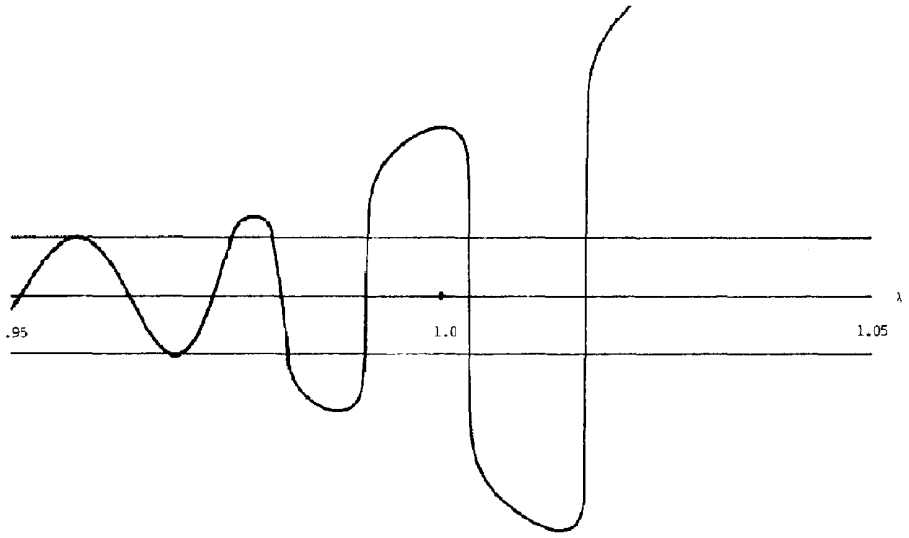

FIG. 28. A part of Fig. 27, drawn at greatly enlarged scale for comparison with later times.

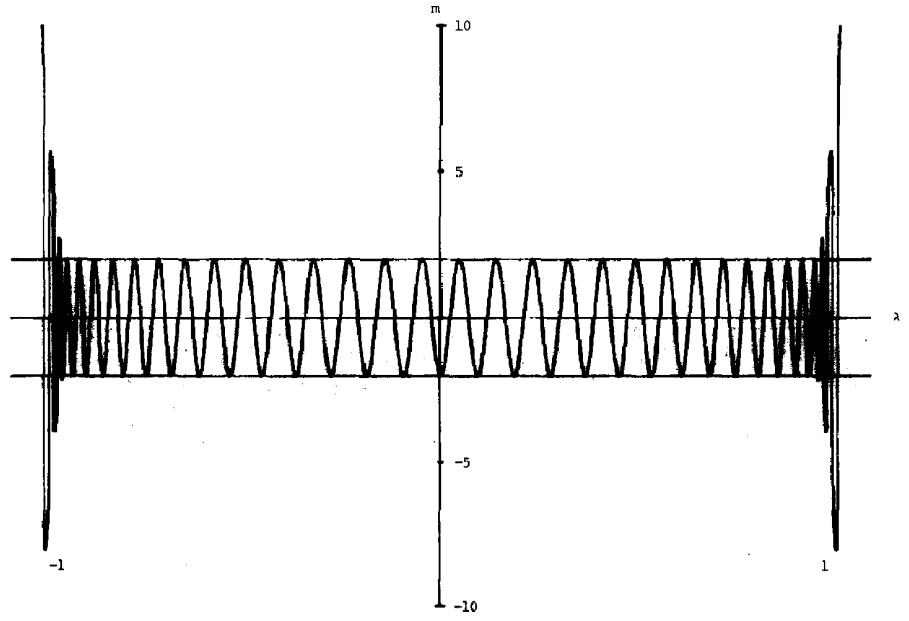

FIG. 29. Modified *Toda* discriminant computed from the solution of the quadratic FPU chain when mode 2 reaches its maximum (cf. Fig. 25). There is no change from Fig. 27 at this scale.

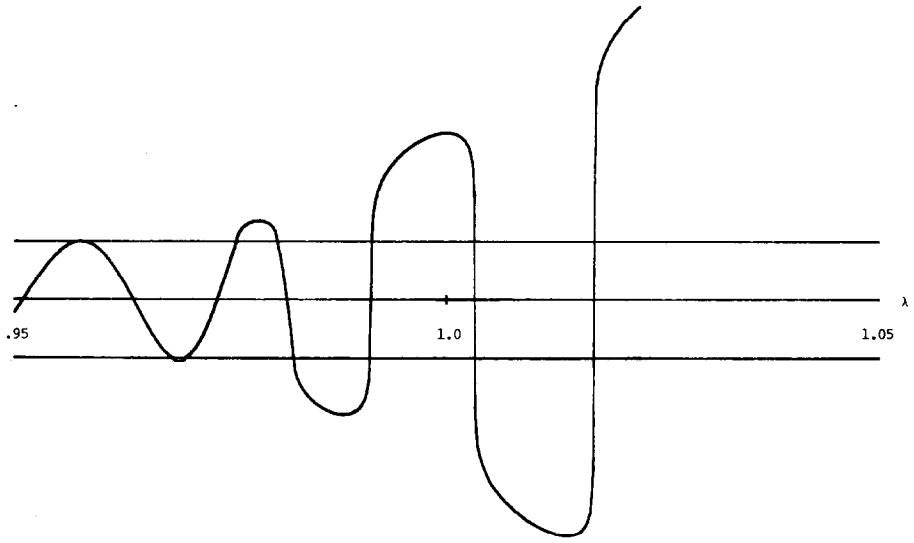

FIG. 30. A part of Fig. 29, drawn at enlarged scale. Figures 28 and 30 are indistinguishable upon superposition.

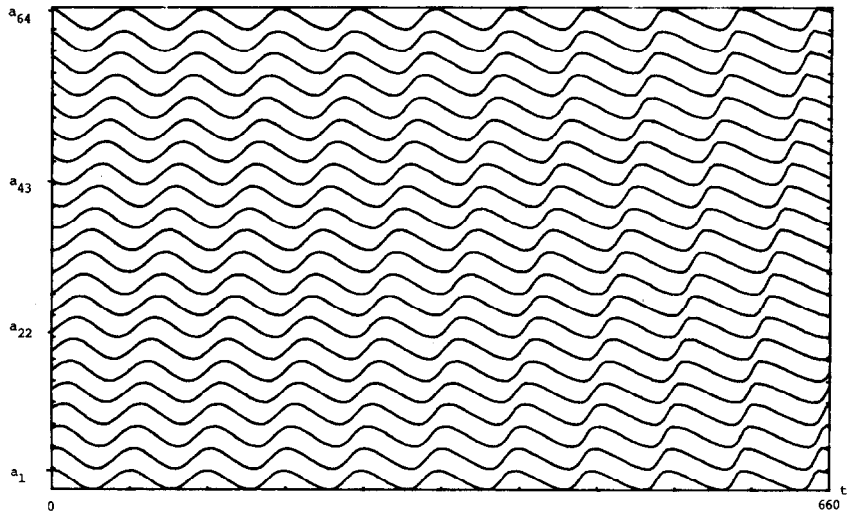

FIG. 31. a_n versus t for the initial condition given by Eq. 6.2, $0 < t < 660$, showing initial steepening of the sine-wave.

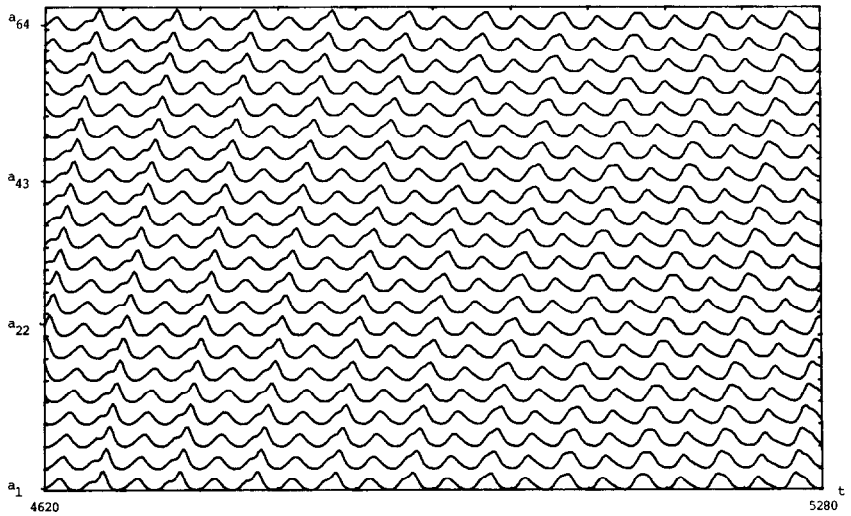

FIG. 32. a_n versus t for the initial condition given by Eq. 6.2, $4620 < t < 5280$, showing separation of some of the pulses predicted by the discriminant.

that are lie symmetrically disposed at $\lambda = \pm 1$. Figure 28 suggests that one will see a left-running soliton, a mixture of soliton-wave packet (that is vague: we imagine it to be a part of a conoidal wave, not quite linear—see Appendix 1), and one linear wave packet. The same type of wave will move toward the right, because of the symmetrical picture at $\lambda = -1$. This is borne out by the timeline plot in Figs. 31, 32, corresponding to an initial condition from which the $\lambda = +1$ part has been removed (see below).

The fact that the Toda action variables remain nearly constant during the integration of the quadratic chain has important ramifications. We must first realize that the Toda action variables will in general change with time, since we are not integrating the equations of motion for the Toda chain. Recall that each phase point (q, p) describing the state of the quadratic chain lies on a (Toda) torus which is characterized by the corresponding graph of the discriminant. Therefore we can visualize the trajectory of the phase point of the quadratic lattice as a curve winding around a torus which is changing with time. If during some interval of time the graph of the discriminant changes slowly, we deduce that the torus also changes slowly. Let us now suppose that the graph of the discriminant describes a state of the chain that is composed of the (nonlinear) superposition of several solitons and near-linear wave packets. As the trajectory of the phase point winds around this slowly changing torus we would expect it to pass through regions which describe states of the chain where each soliton is clearly visible. More generally, if the graph of the discriminant changes only slowly over a sufficiently long period of time, then we should be able to observe the slowly changing solitons and near-linear wave packets described by the discriminant.

To illustrate this situation let us again consider the time evolution of the 66-mass periodic quadratic chain starting from the initial condition

$$q_n = \frac{1}{2}\sin(\pi n/33), \qquad q_n' = -\frac{\omega_1}{2}\cos(\pi n/33) \qquad \text{for} \quad n = 1,\ldots, 66, \tag{6.2}$$

where

$$\omega_1 = 2\sin(\pi/66).$$

Recall that if the chain were linear, the initial condition used by Fermi, Pasta and Ulam would consist of a left-running and a right-running sinusoidal wave; the initial condition above gives rise to the right-running sinusoidal wave. The graph of the

$0 < t < 10{,}000$ the graph of the discriminant changes slowly; therefore we should expect to see the two solitons and several near-linear wave packets predicted by the graph of the discriminant. As seen in Fig. 31 we find that the sinusoidal wave does indeed propagate to the right while it gradually steepens. In Fig. 32, we see that the two solitons and near-linear wave packets, which were superimposed initially, have separated.

A similar experiment on the quadratic chain was performed by Zabusky [11]. The results of this experiment suggested to Zabusky the existence of a new kind of soliton in the quadratic chain, the so-called "lattice-soliton." We argue below that the "lattice-soliton" observed by Zabusky could equally well be interpreted as a near linear wave packet. Unfortunately we cannot directly use the discriminant to analyze Zabusky's experiment, because we were unable to extract the relevant parameter values from his paper. With this apology, let us now present our version of Zabusky's experiment.

Consider the time evolution of the 200-mass periodic quadratic chain starting from the initial condition

$$q_n = \frac{100}{\pi^2}\sin(2\pi n/200), \quad p_n = -2[\exp(\Delta q_n/2) - 1] \quad \text{for} \quad n = 1,\ldots, 200. \tag{7.3}$$

The plot of the discriminant (Figs. 33 and 34) suggests that one should observe 19 solitons and 26 near-linear wave packets, the velocity of the fastest soliton being 1.11 and the group speed of the slowest near-linear wave packet being 0.76. These velocity ranges agree reasonably well with those measured by Zabusky (cf. Fig. 4 and accompanying table in [11]). Furthermore, Zabusky found that his initial sinusoidal wave broke up into 46 pulses, of which 20 had speeds greater than 1. We therefore argue that, to a reasonable degree of accuracy, the results observed by Zabusky could have been predicted by discriminant analysis. In particular, it appears that the "lattice-

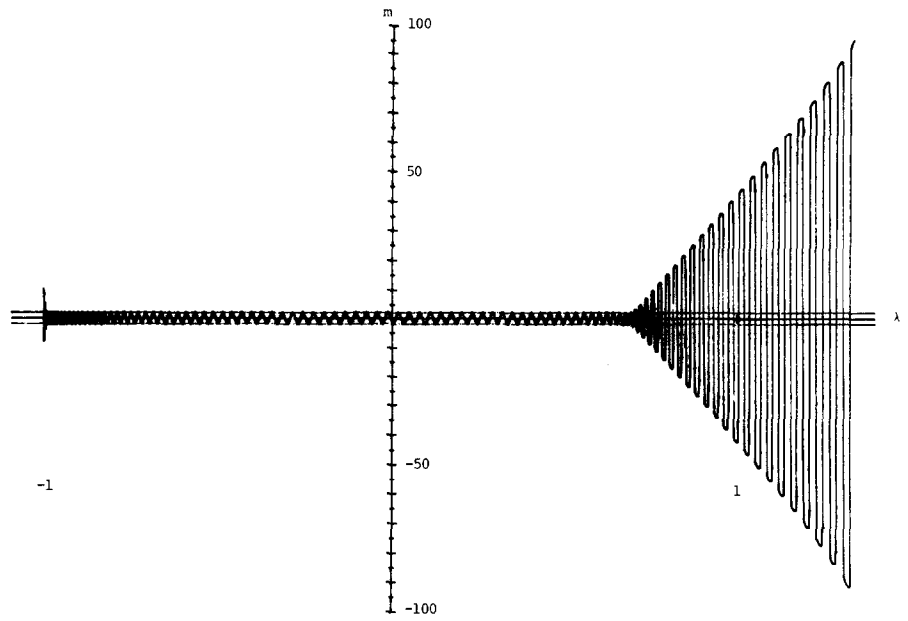

FIG. 33. Modified *Toda* discriminant for the Zabusky-type initial condition (7.2).

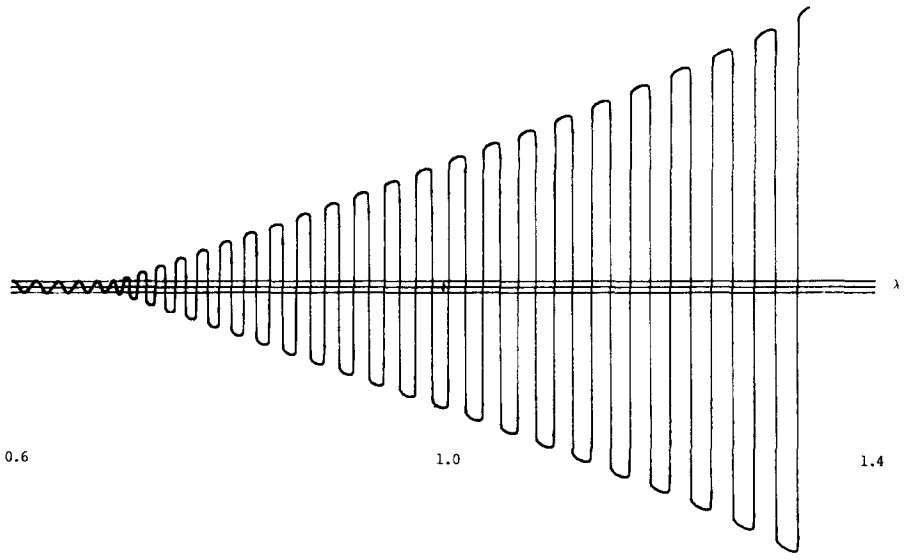

FIG. 34. Part of Fig. 33 drawn at enlarged scale. This permits approximate computation of soliton or group-packet speeds (see text).

solitons" observed by Zabusky were nothing more than the near-linear wave packets of the Toda chain.

After reading a draft of this paper, Prof. Zabusky pointed out some possible defects in our interpretation. He feels that solitons are distinguished by (a) undergoing a phase shift upon interaction, and (b) recurring to their initial position. Linear wave-packets should interact without phase shift, and disperse.

We feel that in an integrable, or near-integrable, chain, recurrence is automatic because of the quasiperiodicity of the motion, and does not require or imply soliton behavior. Likewise, true dispersion becomes impossible, because the wave-packets are constantly forced to interact. We cannot, in our framework, ask whether one of the near-linear packets would disperse if it were left alone. As Example 5, Section 5 shows, adding masses at rest changes the nature of the action variables, and may, for all we know, convert an "inside $|\lambda| = 1$ bump" to an "outside $|\lambda| = 1$ bump," i.e., a linear wave to a soliton.

This leaves the phase shifts to be checked, and we have not done such a calculation. The problem is therefore left unresolved. Our interpretation of the L-solitons observed by Zabusky as near-linear waves rests on two assumptions:

(a) Extrapolation of the soliton-ringing distinction of the infinite Toda chain: we assume, supported to some extent by the practice problems, that a similar distinction prevails in some periodic chain motions. See, for example, the fitting of linear group velocity in Example 6, Section 5.

(b) The infinite Toda chain supports no solitons moving with speed <1; we assume that the same is true of periodic Toda chains, or near-Toda chains.

These arguments are not proofs, of course, and the "true nature" of Zabusky's L-solitons may be very hard to pin down. They live in a domain where infinite-chain concepts do not apply to a periodic chain, nor linear concepts to a nonlinear situation rules are largely empirical, and may well only provide parts of the answer. A convincing explanation of Zabusky's experiment is, therefore, still a problem for the future.

7. Toda Chain with a Light Mass

Our discussion up to this point has dealt exclusively with the unit-mass Toda chain. In this section, we describe some experiments on Toda chains with a mass impurity. The springs obey the same force law as before, masses 2 to N are still unit masses, while mass 1 (the "impurity") is lighter or heavier than the rest.

It is known that the unequal-mass Toda equations are not completely integrable: not all trajectories lie on invariant tori, and there are regions in phase space in which the motion is extremely erratic ("stochastic"). Computer evidence of stochasticity was obtained by Casati and Ford [20], and a rigorous description of the erratic

trajectories at high energy was provided by Bogoyavlenskii [21]. Our experiments deal only with fairly regular motions of an unequal-mass chain. This, of course, is because we want to adapt, as far as is possible, the discriminant analysis of the earlier sections to perturbations of the integrable Toda equations.

Let us outline our approach. We have explained in Sections 3 and 4 that each phase point (q, p) describing a state of the chain lies on a certain torus. The general characteristics of this torus, and hence of the physical shape of the chain, can be seen from the graph of the discriminant (after the change of variables $(q, p) \to (a, b)$). It is now important to note that the values of the masses do not enter into the change of variables, nor into the definition of the discriminant. The fact that all masses are equal to unity becomes important only in the dynamics of the chain. For the equal-mass chain, a phase point stays on the same Toda torus for all time. This is crucial to our analysis, because the discriminant does not tell us *where* on the torus a given phase point lies. So, for example, if the discriminant predicts two solitons and near-linear wave packets of certain group speeds it may well take some time until all these components have separated and have become distinguishable in the chain itself. The implication for the unequal-mass chain is clear. First of all, the equal mass constants of motion are no longer constant when impurities are present. Therefore, the discriminant will change with time. We can always tell, from the graph of the discriminant, on which torus the phase point happens to be at any given time. If,

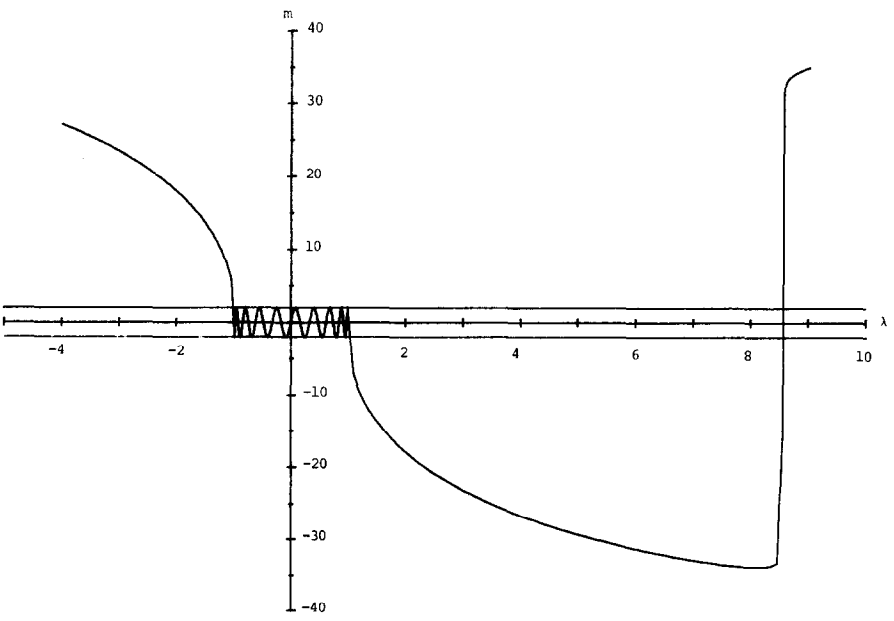

FIG. 35. Modified discriminant for Fig. 39 at the initial time, $t = 0$.

however, the discriminant (and hence the torus) changes very quickly, we cannot deduce anything about the shape of the chain: the components which are "present" in the solution at one time may not have a chance to separate and to become identifiable before the torus has changed so much that the composition of the solution is entirely different. Conversely, if the discriminant changes only gradually over a sufficiently long time interval, we may expect to read off from the discriminant some significant features of the solution—for example, a soliton of slowly changing amplitude, etc.

Consider, as illustration, the sequence of discriminants shown in Figs. 35–38. A single soliton of speed 3, initially centered on an $N = 20$ chain, is sent toward the light mass whose mass is $m = 0.1$. The discriminant undergoes drastic contortions during the time of interaction with the light mass during the time interval $2.5 < t < 3.3$. After that, there is relatively little change (until the soliton has circled the periodic chain and hits the light mass again; this is not shown). The discriminant at $t = 3.5$ shows three solitons; the original one, transmitted with some loss of speed, a much smaller reflected one, and a second transmitted one. There is also some miscellaneous ringing. The three solitons are visible, to varying degrees, on the corresponding time-line plot in Fig. 39. Without the benefit of the discriminant, it

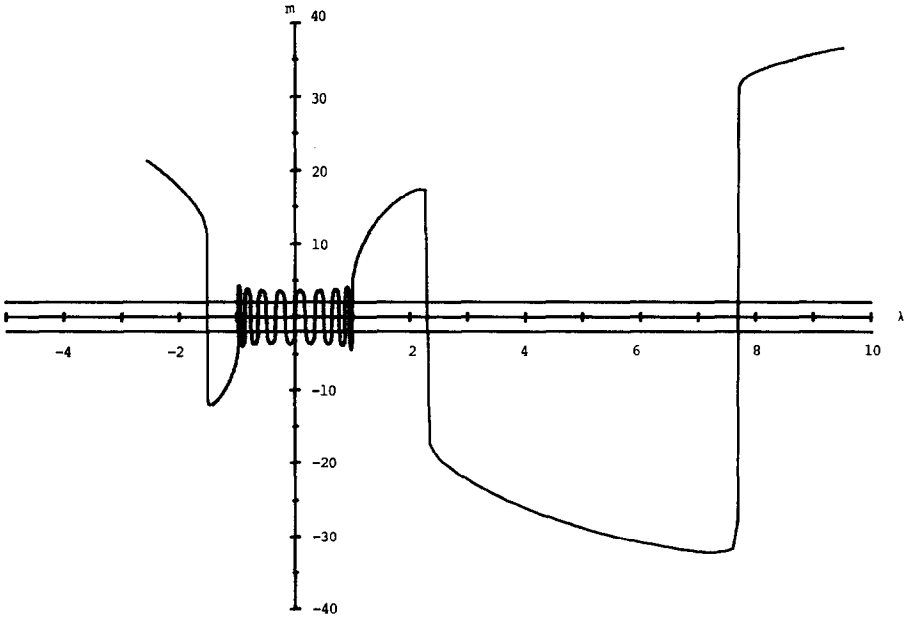

FIG. 36. Modified discriminant for Fig. 39 at $t = 2.65$; the interaction started to change the original discriminant shape at $t = 2.50$.

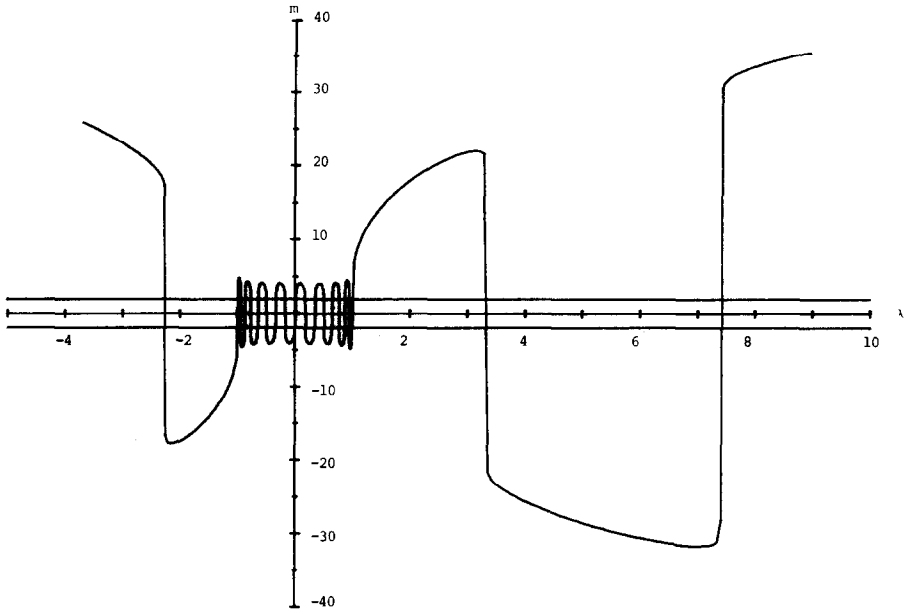

FIG. 37. Modified discriminant for Fig. 37 at $t = 2.70$. Note the extreme change in the three soliton actions during the short interval from $t = 2.65$ to $t = 2.70$; in particular, the large second action.

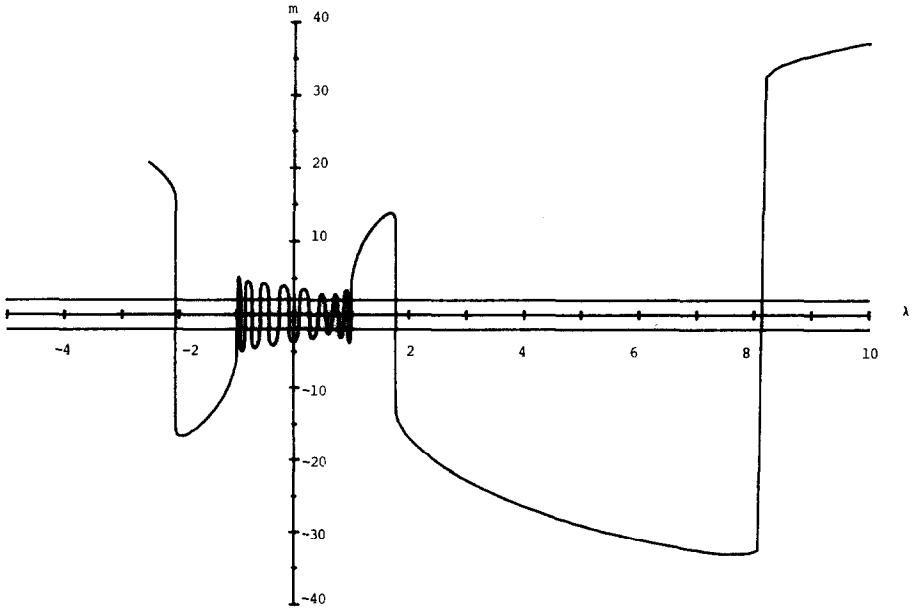

FIG. 38. Modified discriminant for Fig. 37 at $t = 3.50$. This picture remains essentially unchanged until the next interaction. Note that the size of the reflected soliton action (bump 23) has increased while the second transmitted soliton action (bump 2) has decreased in comparison with Fig. 37.

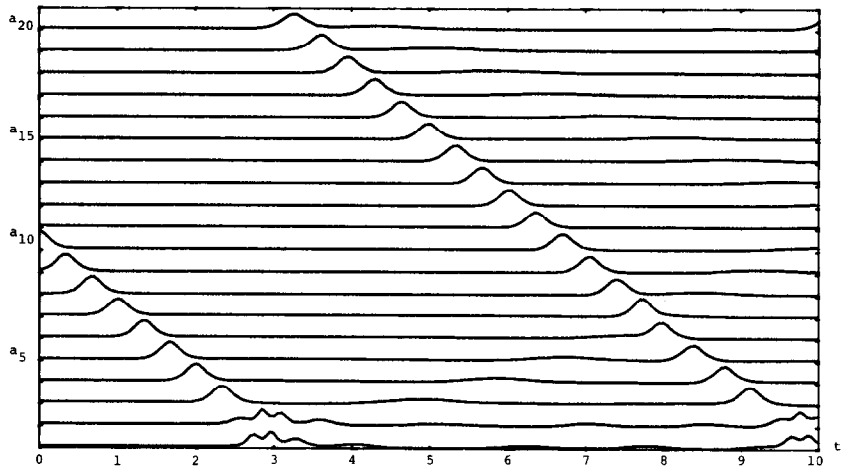

FIG. 39. a_n versus t plot for a soliton of speed 3 impinging on a light-mass impurity on an $N = 20$ chain. The light mass is $m = 0.1$ (MINV $= 1/m = 10$); its timeline is the bottom one. There is considerable oscillation that remains localized at the impurity.

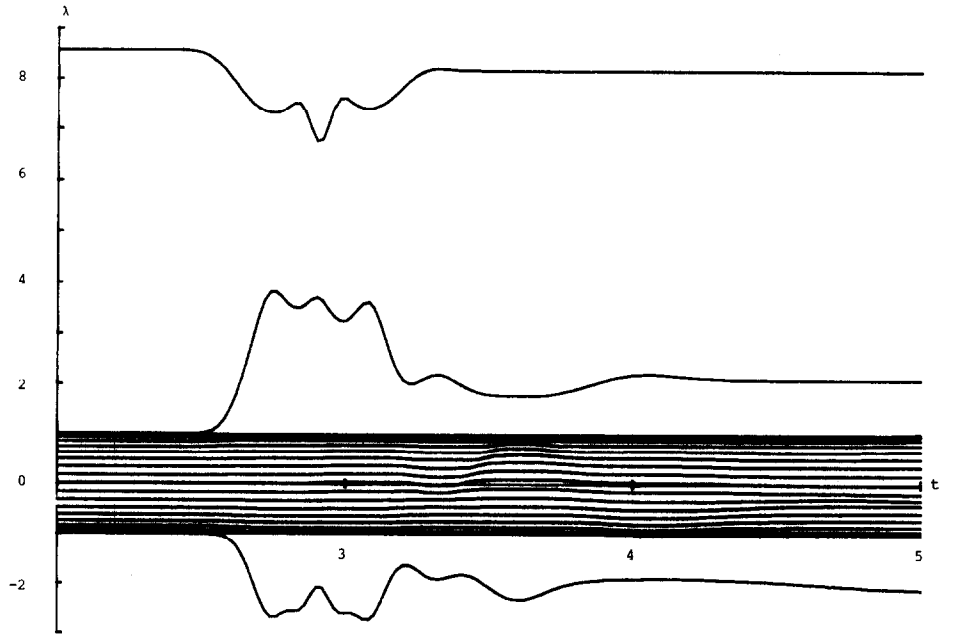

FIG. 40. Plot of the roots of $\Delta(\lambda) = 0$ as function of time, for the run of Fig. 39.

would not be at all easy to distinguish the second transmitted soliton from near-linear wave-packets. Figure 40 summarizes the changes in the discriminant by displaying the graphs of the 20 roots of the discriminant as functions of time. One can see there the emergence of two of the roots from the interval $[-1, +1]$; they, of course, correspond to the soliton-type bumps seen in Fig. 39.

We now come to the main observation of this section. One usually studies linear chains in terms of Fourier modes, and near-linear chains by following the time-evolution of the Fourier amplitudes, which in the linear case were constant and uncoupled. If the nonlinearity is small, one generally finds that a dominant mode becomes coupled to just a few side-bands; a typical first approximation is to take the dominant mode to be coupled to two of its harmonics, and this leads to the familiar three-mode interactions. The analog of this procedure for perturbed equal-mass Toda chains would be to follow the time-variation and coupling the Toda action variables. The discriminant pictures in Figs. 35–38 show some of the mode-coupling mechanism in the particular problem studied. The dominant action variable, corresponding to the incident soliton, is coupled almost exclusively to two others; it can be seen very clearly in Fig. 40 how the "energy" of these modes is transferred and used to excite the reflected soliton mode.

We now have a use for the discriminant at all times, even during the short interval

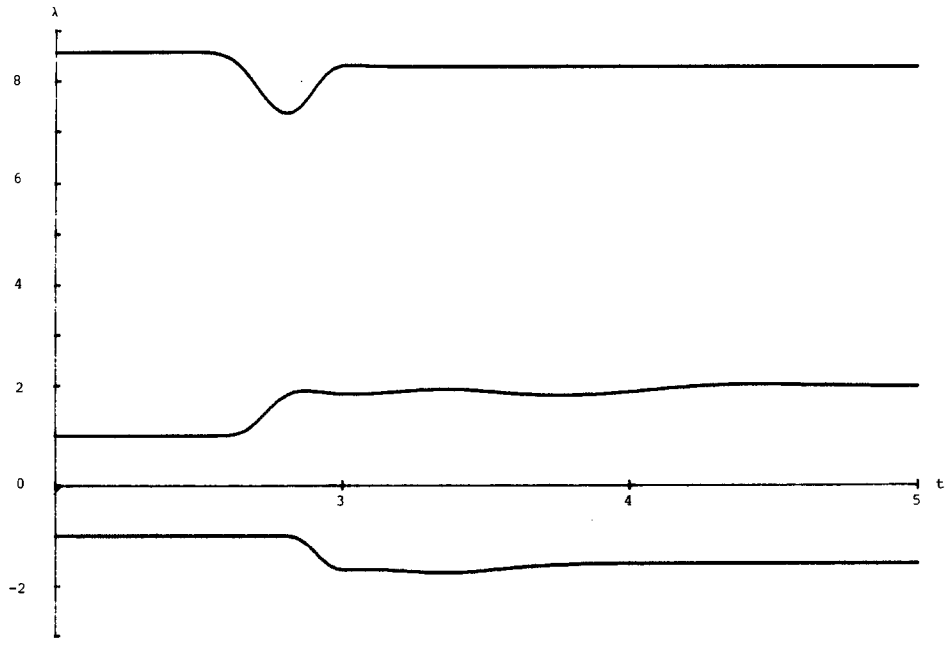

FIG. 41. Plot of the roots λ_1, λ_2, λ_{20} of $\Delta(\lambda) = 0$ versus time, for light mass $1/m = 1.5$.

when it changes very rapidly. Before and after the soliton-impurity interaction, the discriminant accurately reflects the shape of the chain. During the interaction, the rapid changes of the discriminant show us the mode-coupling by which new action variables are excited.

Figures 41–42 display the time-evolution of the roots λ_i of the discriminant, for $i = 1, 2$, and 20, for other values of the light mass ($MINV = 1/m$); the other parameters are the same as in Fig. 37. It is interesting that the mode-coupling gyrations become more violent as the light mass decreases. The corresponding plot for a heavy impurity is totally different (Fig. 43); one can imagine the heavy mass, once set into motion, knocking out several solitons by repeated impulses to the rest of the chain. This was already observed in [22, 23].

Our results complement those obtained from soliton perturbation theory. In this method (initiated by Kaup [24], see also Kaup and Newell [25]), approximate equations for the time-evolution of normally constant scattering data are derived. The techniques were used by Yajima [26] to study precisely the soliton–light mass interaction. It is a basic feature of the soliton-perturbation theory that the number of solitons present in the perturbed solution is assumed to be constant. In the light mass problem, it would be postulated that there is, at all times, a single soliton; the perturbation theory would try to follow its change of speed as caused by the emergence of

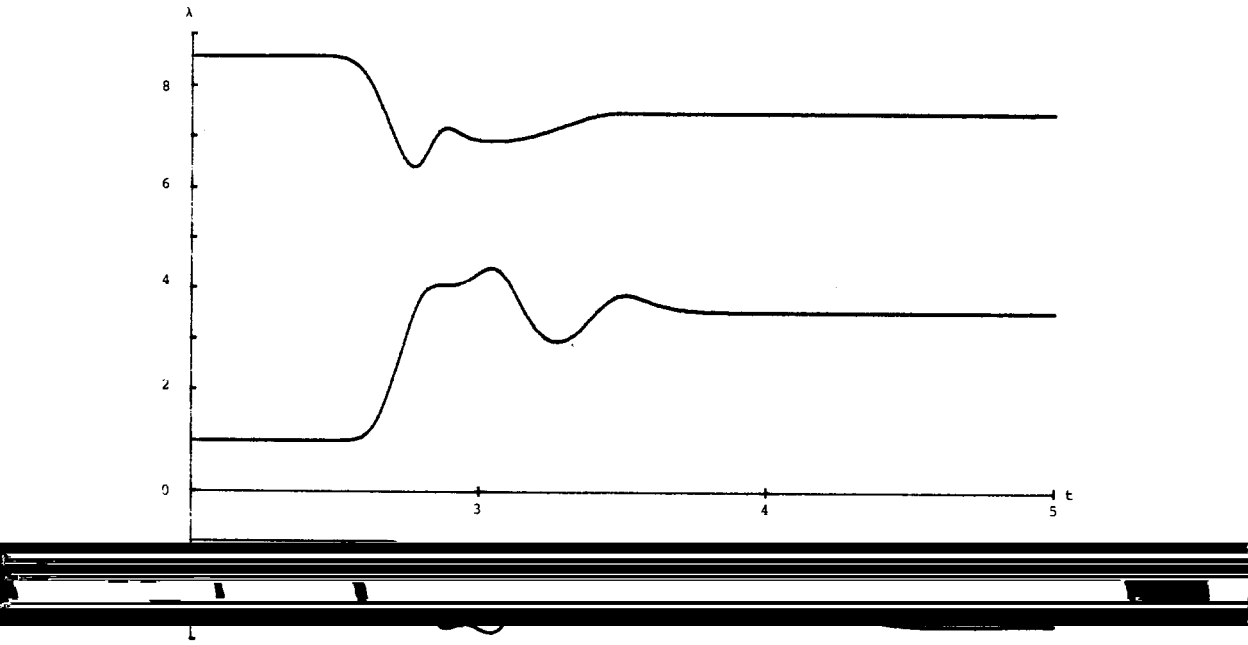

FIG. 42. Plot of the roots λ_1, λ_2, λ_{20} of $\Delta(\lambda) = 0$ versus time, for a light mass $1/m = 3$.

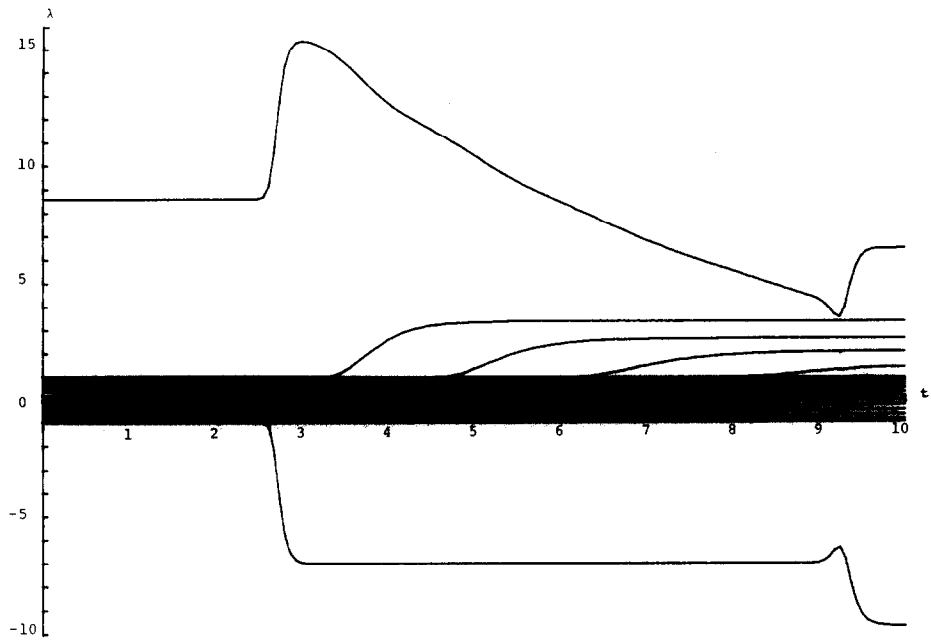

FIG. 43. Plot of all roots of $\Delta(\lambda) = 0$ for the case of a heavy mass ($m = 10$).

ringing (action variables inside $[-1, +1]$). It is clear from our discriminant plots that this assumption requires a value of *MINV* extremely close to 1. On the other hand, our pictures suggest that a much better theory, valid over long time intervals, need not be more complicated: the interaction process basically involves three solitons, and one must "only" derive equations which will describe the transfer of energy from the incident one to the other two. The ringing component of the solution should, to a good approximation, be completely negligible.

The creation or destruction of solitons by a perturbation has hardly been treated analytically; we only know of some unpublished results of Yajima and of McLaughlin and Overman, and neither of these methods is sophisticated enough to handle the light mass perturbation. It would be interesting to see the three-mode interaction suggested by our computations put on a firmer analytical footing.

APPENDIX 1

We collect certain formulas for the traveling-wave solutions of the Toda chain. Some of these may be found in the literature [1, 16]. Others appear to be new and are useful for the numerical study of the basic Toda modes.

Let

$$\theta(z;q)=\sum_{n=-\infty}^{\infty}(-1)^n q^{n^2}\exp(2\pi inz),\qquad 0<q<1; \tag{A.1}$$

this is a Jacobi θ-function. The traveling-wave solutions are derived from θ by the formula

$$p_n=\frac{d}{dt}\ln\left(\frac{\theta(z_n)}{\theta(z_{n+1})}\right), \tag{A.2}$$

where

$$z_n=\frac{kn-\omega t}{2\pi}+\delta\qquad(\delta=\text{constant}).$$

The wavenumber k takes on one of the values

$$k_j=\frac{2\pi j}{N},\qquad j=1,\ldots,N, \tag{A.3}$$

and the frequency ω_j is connected with k_j and with the modulus q of the θ-function (an amplitude parameter) by the nonlinear dispersion relation

$$\omega_j^2=-4\pi^2\left\{\frac{d^2}{dz^2}\ln[\theta(z;q)]\right\}^{-1},\qquad z=\frac{k_j}{2\pi}-\frac{1}{2}\ln(q) \tag{A.4}$$

Two limits of these formulas are of interest:

Case 1. $q\to 0$ (the harmonic limit). Transformations of the θ-functions lead to a formula equivalent to (A.2),

$$p_n(t)=-4\omega\sum_{l=1}^{\infty}\frac{q^l}{1-q^{2l}}\sin(kl/2)\cos(l(kn-\omega t+\delta)), \tag{A.2'}$$

where k is of the form (A.3) and k, ω, q are related by

$$\omega^{-2}=(2\sin(k/2))^{-2}-2\sum_{l=1}^{\infty}\left(\frac{lq^{2l}}{1-q^{2l}}\right)\cos(kl), \tag{A.4'}$$

which is equivalent to (A.4), being obtained from that relation after some manipulation.

As $q\to 0$, we obtain from (A.2') and (A.4'):

$$p_n(t)=-2q\omega^2\cos(kn-\omega t+\delta)+O(q^2),$$
$$\omega=2\sin(k/2)+O(q^2);$$

the limit is therefore the harmonic normal mode with a small amplitude measured by q.

Case 2. $q \to \infty$ (the soliton limit). It is convenient to transform (A.2) and (A.4) once again.

$$p_n(t) = 2\Omega \sinh(\gamma) \sum_{l=-\infty}^{\infty} \{\cosh(\gamma) + \cosh(2\gamma(N - \mu t) + \gamma - 4Ql)\}^{-1} \tag{A.2''}$$

$$\Omega^{-2} = Q^{-1} + \sum_{l=-\infty}^{\infty} \sinh^{-2}(\gamma - 2Ql), \tag{A.4''}$$

where the parameters are

$$Q = -\pi^2/[2 \ln(q)],$$
$$\mu = \omega/k,$$
$$\gamma = Qk/\pi,$$
$$\Omega = Q\omega/\pi.$$

As $q \to 1$, $Q \to \infty$; let $k \to 0$ with γ fixed. Then $\Omega \to \sinh(\gamma)$, and (A.2'') reduces to the momentum for a single soliton on the infinite chain,

$$p_n(t) = \frac{2 \sinh^2(\gamma)}{\cosh(\gamma) + \cosh\left[2\gamma\left(n - n_0 - \dfrac{\sinh(\gamma)}{\gamma} t\right)\right]}.$$

APPENDIX 2

The computations presented in this paper were performed on a Data General Eclipse $S/230$. The algorithms were coded in FORTRAN V using double precision floating point arithmetic; this arithmetic offers numbers having 16 decimal digits of accuracy and a dynamic range of $10^{\pm 75}$.

Each experiment in this paper involved one or more of the following three steps:

(1) Integrate the equations of motion,

(2) plot the discriminant Δ which corresponds to a prescribed point (q, p) in phase-space, and

(3) compute a point (q, p) in phase-space which corresponds to a prescribed discriminant Δ.

Let us now describe briefly the computational algorithms used in each of these steps.

The equations of motion (4.4) for the Toda chain were integrated using RKF45

[27]. A typical integration for the 25-mass Toda chain ran from $t = 0$ to $t = 50$ with the error tolerances used by RKF45 set at 10^{-6}; such an integration took 10 CPU seconds. The equations of motion (4.1, 6.1) for the quadratic chain were also integrated using RKF45. The integration of the 66-mass quadratic chain ran from $t = 0$ to $t = 10{,}560$ with the error tolerances used by RKF45 set at 10^{-9}; this integration took 10,000 CPU seconds. To save CPU time on these integrations one might choose to replace RKF45 by the Bulirsch–Stoer code DIFSUB [28]; note that the simplicity of the equations of motion (4.4) would probably make multistep methods such as the Adams code [29] inefficient.

Plots of the discriminant Δ were obtained by using a simple recurrence relation to compute $\Delta(\lambda)$ given λ. For an N-mass periodic Toda lattice it is known [14] that

$$\Delta(\lambda) = y_N^{(0)}(\lambda) + y_{N+1}^{(1)}(\lambda),$$

where $y^{(0)}$ and $y^{(1)}$ are the solutions of the difference equation ($a_0 = a_N$)

$$a_{n-1}\, y_{n-1}(\lambda) + b_n\, y_n(\lambda) + a_n\, y_{n+1}(\lambda) = \lambda y_n(\lambda)$$

defined by the initial conditions

$$y_0^{(0)} = 1, \qquad y_1^{(0)} = 0,$$
$$y_0^{(1)} = 0, \qquad y_1^{(1)} = 1.$$

The discriminant Δ for this N-mass chain has exactly $N - 1$ extrema.

It can be seen from the plots of the discriminant presented in this paper that the typical discriminant graph has very rapid oscillations, very steep segments, and also some very broad bumps. If one were to try to resolve all these features by plotting $\Delta(\lambda)$ at a very dense mesh of λ's (say 1000 per graph), it would be exceedingly time-consuming to obtain each plot.

To ensure that the computed graph of λ reproduces the shape, height, and location of each of these extrema accurately, we used the following procedure. First, employ the EISPACK routines [30] to compute the eigenvalues $\mu_1 > \mu_2 > \cdots > \mu_{N-1}$ of the tridiagonal matrix

$$M = \begin{bmatrix} b_1 & a_1 & & & 0 \\ a_1 & b_2 & a_2 & & \\ & & \cdots & & \\ & & a_{N-3} & a_{N-2} & a_{N-2} \\ 0 & & & a_{N-2} & b_{N-1} \end{bmatrix} \tag{A.5}$$

obtained by deleting the last row and column from the periodic Jacobi matrix L in (4.5). Second, use Gerschgorin's theorem [31] to compute upper and lower bounds $\mu_0 > \mu_N$ for the eigenvalues of L. It is known [9] that

$$(-1)^n \Delta(\mu_n) \geqslant 2 \qquad \text{for} \quad n = 0, \ldots, N.$$

Each interval $[\mu_{j+1}, \mu_j]$ therefore contains at most two extrema of Δ. Having localized the extrema, we can get the important characteristics of Δ by plotting $\Delta(\lambda)$ at just 10 or so λ's in each interval $[\mu_{j+1}, \mu_j]$. This results in a saving of both time and storage.

Alternatively, one might try to pin down the location of the extrema of Δ by computing the roots of $\Delta = 2$, i.e., the eigenvalues $\lambda_1, \ldots, \lambda_N$ of L. These numbers would also be necessary for the numerical computation of the action variables (cf. Section 5). It is not difficult to compute the eigenvalues of L: if S is the permutation matrix that makes the rows 1, 2, 3, 4,... of SL correspond to the rows 1, N, 2, $N-1$,... of L then

$$K = SLS^T$$

is a pentadiagonal matrix [32] that is orthogonally similar to L; therefore the eigenvalues of L and K are identical. The eigenvalues of K can now be economically determined since the EISPACK routines [30] can be used to reduce K to tridiagonal form.

It would be possible also to use the penta-diagonal matrix K to compute the characteristic polynomial of L (and hence Δ) in a very stable way (using Gauss elimination with partial pivoting), avoiding the overflow or underflow sometimes associated with the use of the recursion relation defining Δ.

The construction of a point (q, p) in phase-space which corresponds to a prescribed discriminant is slightly more complicated. We refer the interested reader to the discussion presented in [9].

ACKNOWLEDGMENTS

We are grateful to Professor N. Zabusky and to an anonymous referee for taking time to read the manuscript very carefully, and for their helpful corrections, suggestions, objections, and criticisms.

REFERENCES

1. M. TODA, (a) *J. Phys. Soc. Japan* **22** (1967), 431; (b) *J. Phys. Soc. Japan* **23** (1967), 501; (c) *J. Phys. Soc. Japan Suppl.* **26** (1969), 235; (d) *Progr. Theor. Phys. Suppl.* **45** (1970), 174; (e) *Phys. Rep.* **18C** (1975), 1.
2. M. HENON, *Phys. Rev. B* **9** (1974), 1921.
3. H. FLASCHKA, *Phys. Rev. B* **9** (1974), 1924; *Progr. Theor. Phys.* **51** (1974), 703.
4. S. V. MANAKNOV, *Soviet Phys. JETP* **40** (1976), 269.
5. B. L. HOLIAN AND G. K. STRAUB, *Phys. Rev. B* **18** (1978), 1593.
6. G. K. STRAUB, B. L. HOLIAN, AND R. G. PETCHEK, *Phys. Rev. B* **19** (1979), 4049.
7. B. HOLIAN, H. FLASCHKA, AND D. W. MCLAUGHLIN, *Phys. Rev. A* **24** (1981), 2595.
8. H. FLASCHKA, in preparation.
9. W. E. FERGUSON, JR., *Math. Comp.* **35** (1980), 1203.
10. E. FERMI, J. PASTA, AND S. ULAM, LASL Report LA-1940 (1955); Reprinted in "Collected Papers of E. Fermi," V.II, Univ. of Chicago Press, 1965, p. 978, and in Lectures in Applied Math., V.15, p. 143, Amer. Math. Soc., R.I., 1974.

11. N. J. ZABUSKY, *Comp. Phys. Comm.* **5** (1973), 1.
12. W. E. FERGUSON, JR., H. FLASCHKA, AND D. W. MCLAUGHLIN, *Kyoto Univ. Lecture Notes* **332** (1978), 171.
13. A. ARNOLD AND A. A. AVEZ, "Ergodic Problems of Classical Mechanics," Benjamin, New York, 1968.
14. H. FLASCHKA AND D. W. MCLAUGHLIN, *Progr. Theor. Phys.* **55** (1976), 438.
15. H. FLASCHKA, *in* "Lecture Notes in Physics" No. 38, p. 441, Springer-Verlag, Berlin/New York, 1975.
16. E. DATE AND S. TANAKA, *Progr. Theor. Phys. Suppl.* **59** (1976), 107.
17. P. VAN MOERBECKE, *Invent. Math.* **30** (1975), 217.
18. H. FLASCHKA AND D. W. MCLAUGHLIN, *in* "Lecture Notes in Math." No. 515, p. 253, Springer-Verlag, Berlin/New York, 1976.
19. E. A. JACKSON, *Rocky Mountain Math. J.* **8** (1978), 127.
20. G. CASATI AND J. FORD, *Phys. Rev. A* **12** (1975), 1702.
21. O. A. BOGOYAVLENSKII, *Comm. Math. Phys.* **51** (1976), 201.
22. A. NAKAMURA AND S. TAKENO, *Progr. Theor. Phys.* **58** (1977), 1074.
23. A. NAKAMURA, *Progr. Theor. Phys.* **59** (1978), 1447.
24. D. J. KAUP, *SIAM J. Appl. Math.* **31** (1976), 121.
25. D. J. KAUP AND A. C. NEWELL, *Proc. Roy. Soc. London A* **361** (1978), 413.
26. N. YAJIMA, *Physica Scripta* **20** (1979), 431.
27. G. E. FORSYTHE, M. A. MALCOLM, AND C. B. MOLER, "Computer Methods for Mathematical Computations," Prentice–Hall, Englewood Cliffs, N.J., 1977.
28. C. W. GEAR, "Numerical Initial Value Problems in Ordinary Differential Equations," Prentice–Hall, Englewood Cliffs, N.J., 1971.
29. [illegible] MOLER, "Matrix Eigensystem Routines—EISPACK Guide," Springer-Verlag, Berlin/New York, 1976.
31. P. LANCASTER, "Theory of Matrices," Academic Press, New York, 1969.
32. G. H. GOLUB AND A. BJORCK, *SIAM Rev.* **19** (1977).